

UNCLASSIFIED

AD NUMBER
AD128957
NEW LIMITATION CHANGE
TO Approved for public release, distribution unlimited
FROM Distribution authorized to U.S. Gov't. agencies and their contractors; Administrative/Operational Use; 8 Oct 1956. Other requests shall be referred to the Naval Ordnance Test Station, China Lake, CA.
AUTHORITY
USNOTS Notice, 27 Jan 1966

THIS PAGE IS UNCLASSIFIED

UNCLASSIFIED

A128957

Armed Services Technical Information Agency

Reproduced by

DOCUMENT SERVICE CENTER

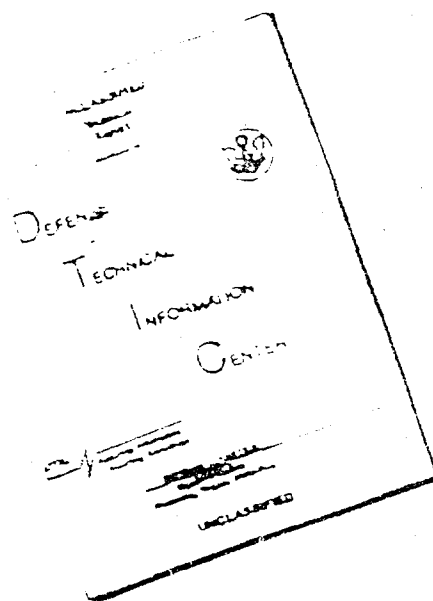
KNOTT BUILDING, DAYTON, 2, OHIO

This document is the property of the United States Government. It is furnished for the duration of the contract and shall be returned when no longer required, or upon recall by ASTIA to the following address: Armed Services Technical Information Agency, Document Service Center, Knott Building, Dayton 2, Ohio.

NOTICE: WHEN GOVERNMENT OR OTHER DRAWINGS, SPECIFICATIONS OR OTHER DATA ARE USED FOR ANY PURPOSE OTHER THAN IN CONNECTION WITH A DEFINITELY RELATED GOVERNMENT PROCUREMENT OPERATION, THE U. S. GOVERNMENT THEREBY INCURS NO RESPONSIBILITY, NOR ANY OBLIGATION WHATSOEVER; AND THE FACT THAT THE GOVERNMENT MAY HAVE FORMULATED, FURNISHED, OR IN ANY WAY SUPPLIED THE SAID DRAWINGS, SPECIFICATIONS, OR OTHER DATA IS NOT TO BE REGARDED BY IMPLICATION OR OTHERWISE AS IN ANY MANNER LICENSING THE HOLDER OR ANY OTHER PERSON OR CORPORATION, OR CONVEYING ANY RIGHTS OR PERMISSION TO MANUFACTURE, USE OR SELL ANY PATENTED INVENTION THAT MAY IN ANY WAY BE RELATED THERETO.

UNCLASSIFIED

DISCLAIMER NOTICE



THIS DOCUMENT IS BEST
QUALITY AVAILABLE. THE COPY
FURNISHED TO DTIC CONTAINED
A SIGNIFICANT NUMBER OF
PAGES WHICH DO NOT
REPRODUCE LEGIBLY.

REPRODUCED FROM
BEST AVAILABLE COPY

CLASSIFIED

57

Information Agency

CENTER
Dayton 2, Ohio

document. It is furnished for the use of the Government, or upon recall by ASTIA, Technical Information Agency, Dayton 2, Ohio.

REPRODUCTIONS OR OTHER DATA
CONTAINED HEREIN WITH A DEFINITELY RELATED
GOVERNMENT THEREBY INCURS
RESPONSIBILITY; AND THE FACT THAT THE
DATA IN ANY WAY SUPPLIED THE
DATA IS TO BE REGARDED BY
THE USER AS THE PROPERTY OF THE
HOLDING THE HOLDER OR ANY OTHER
OR PERMISSION TO MANUFACTURE,
IN ANY WAY BE RELATED THERETO.

CLASSIFIED

AD No 128957

ASTIA FILE COPY

FC

NAV

This publication has been reviewed in accordance with OPNAVINST 5510.7. The security classification shown is correct for the full document. When separate, the abstract is UNCLASSIFIED; the title is UNCLASSIFIED.

2 May 1952
(Date)

Madeline Worling
Technical Information Department
U.S. Naval Ordnance Test Station

AD No 128957
ASTIA FILE COPY

FC

NAVORD REPORT

This publication has been reviewed in accordance with OPNAVINST 5510.7. The security classification shown is correct for the full document. When separate, the abstract is UNCLASSIFIED; the title is UNCLASSIFIED.

2 May 1952
(Date)

Nadine Werling
Technical Information Department
U.S. Naval Ordnance Test Station



U N C L A S S I F I E D

U. S. NAVAL ORDNANCE TEST STATION

F. L. Ashworth, Capt., USN
Commander

Wm. B. McLean, Ph.D.
Technical Director

NOTS 1597

NAVORD REPORT 5365

Part 1

WATER-ENTRY CAVITY MODELING

Part 1, Vertical Cavities

By

J. G. Waugh

and

G. W. Stubstad

Underwater Ordnance Department

This report, published by the Underwater Ordnance Department, is the approved version of 807/MS-96. It consists of cover, 28 leaves and abstract cards. From the original printing of 100 copies, this document is

Copy No. 32

Naval Lake, California

8 October 1956

U N C L A S S I F I E D

FOREWORD

This report contains the results of a modeling study on missiles launched vertically into the Variable-Angle Variable-Pressure Launching Tank at the U. S. Naval Ordnance Test Station. The study was made under Bureau of Ordnance Task Assignment NOTS-C3d-444-3-56.

Another study on the results of modeling with missiles launched at oblique angles is contained in Part 2 of this report.

This report was reviewed for technical accuracy by J. H. Wayland of the California Institute of Technology and by T. G. Lang of this Station.

D. J. WILCOX, Head
Underwater Ordnance
Department

Released under
the authority of:

WM. B. McLEAN
Technical Director

ABSTRACT

Modeling studies were conducted with a 2-inch-diameter hemisphere-head missile as a prototype and with 1- and 1/2-inch-diameter models of the prototype. This "modeling with models" program was carried out to investigate the importance of gas-density scaling in conjunction with Froude and cavitation-number scaling in water-entry cavity modeling.

The observation of the cavities formed by the vertical entry of these models showed that one-to-one scaling of the Froude and cavitation numbers and of the gas density coefficient modeled the cavity to a high degree of accuracy. Failure to scale the cavitation number did not prevent good modeling, but when the gas density coefficient was not scaled modeling did not occur. Good water-penetration-distance modeling obtained for all modeling conditions.

Evaluation of the importance of atmospheric-density scaling on water-entry modeling must be deferred until tests are extended to include launchings of models at oblique angles.

Cavitation-number scaling cannot be disregarded in the general water-entry modeling problem because it has been found necessary to model missile motion in oblique water entry.

CONTENTS

Foreword	iii
Abstract	iv
Introduction	1
Water-Entry Cavity Modeling Technique	2
Experimental Program	3
Prototype and Models	3
Launching Facilities	4
Test Conditions	4
Discussion of Results	9
Cavity Closure	17
Cavity Diameter	18
Cavity Volume From Projected Cavity Area	18
Missile Motion in Underwater Cavity	21
Scaling of Full-Size Missiles	25
Conclusions	29
Appendixes:	
A. Prediction of Cavity Pressure From Cavity Shape	31
B. Origin of Circular Striae on Water-Entry Cavity	41
Nomenclature	46
References	48

INTRODUCTION

An important objective in small-scale modeling of the water entry of bombs, torpedoes, and other projectiles is to determine the underwater trajectory of the prototype missile. The initial regime of underwater trajectory motion at high water-entry speeds takes place with a cavity. It is evident that cavity size and shape affect the underwater-trajectory behavior of the missile. Hence successful modeling of underwater trajectory in cavity motion necessarily includes modeling of the cavity.

In modeling studies with one-to-one Froude and cavitation-number scaling (with reduced air pressure), the air density is not preserved. This technique scales static pressure on the water and cavity surfaces to the extent that pressure is constant over connected regions of air, but it does not scale the dynamic pressure, $\frac{1}{2}\rho v^2$. Consequently, reducing the air density lessens the pressure tending to close the cavity and delays cavity seal. This may increase cavity size by allowing a larger volume of air to enter the cavity. Therefore, in order to model the cavity size it may become necessary to preserve gas density.

Good water-entry and underwater-trajectory modeling (Ref. 1-3) have been obtained for several missile configurations with one-to-one Froude and cavitation-number scaling. This was accomplished in the Controlled-Atmosphere Launching Tank at the California Institute of Technology and in the Variable-Angle Variable-Pressure Launching Tank at the U.S. Naval Ordnance Test Station (NOTS). Since no data were obtained on cavity size and shape, the role of the cavity in determining missile performance is not clear, and the sensitivity of the cavity to the scaling conditions is not known.

The purpose of the experimental program reported here was to investigate the importance of gas-density scaling in conjunction with Froude and cavitation-number scaling in water-entry cavity modeling. Since no large-scale prototype data were available, and time and expense precluded obtaining them, it was decided to conduct a "modeling with models" program in which a 2-inch diameter model was used as the prototype missile. The results of these studies could be used to evaluate the feasibility of modeling with larger scaling ratios which are required for modeling a prototype service missile.

WATER-ENTRY CAVITY MODELING TECHNIQUE

Water-entry theory (Ref. 4 and 5) indicates that with one-to-one Froude and cavitation-number and gas-density scaling, the water-entry cavity may be properly modeled and missile space-time similitude obtained. The theory will not be presented here, but the model constraints and the model-prototype relationships derived from theory on the basis that water is used for both model and prototype are as follows:

Let the ratio of the model diameter to the prototype diameter (modeling scale factor) be given by

$$(1) \quad \lambda = \frac{d_m}{d_p}$$

The model constraints are

$$(2) \quad l_m = \lambda l_p$$

$$(3) \quad m_m = \lambda^3 m_p$$

$$(4) \quad I_m = \lambda^5 I_p$$

The atmospheric-pressure modeling constraint is

$$(5) \quad P_{gm} = \lambda P_{gp}$$

The gas-density modeling constraint is

$$(6) \quad \rho_{gm} = \rho_{gp}$$

Corresponding points along the geometrically similar trajectories are identified by equal distances in diameters or calibers:

$$(7) \quad s_m = \frac{d_m}{d_p} s_p = \lambda s_p$$

The time similitude gives

$$(8) \quad t_m(s_m) = \sqrt{\lambda} t_p(s_p)$$

or

$$(9) \quad s_m(t_m) = \lambda s_p(t_p)$$

where t_m and t_p are the model and prototype times for corresponding points. At the instant of missile water contact $t_m = t_p = 0$ and $s_m(0) = s_p(0) = 0$.

Other model-prototype relationships are as follows:

$$(10) \quad v_m(t_m) = \sqrt{\lambda} v_p(t_p)$$

$$(11) \quad \xi_m(t_m) = \xi_p(t_p)$$

$$(12) \quad \theta_m(t_m) = \theta_p(t_p)$$

$$(13) \quad a_m(t_m) = a_p(t_p)$$

$$(14) \quad \psi_m(t_m) = \psi_p(t_p)$$

Launching constraints on model orientation and velocity are given by Eq. 10 to 14, since the initial boundary (water-contact) conditions must satisfy these equations. For proper water-entry cavity modeling, geometric similarity will obtain with linear dimensions of the model cavity scaling as λ at time $\sqrt{\lambda} t$.

EXPERIMENTAL PROGRAM

PROTOTYPE AND MODELS

A simple shape consisting of a hemispherical head, cylindrical body section, and canther tail was used for the modeling studies. The hemispherical head shape was selected for several reasons. First, it was known from previous investigations (Ref. 6 and 7) that change in atmospheric density caused large differences in the vertical water-entry cavity of a sphere. Therefore it was expected that changes in atmospheric density would produce measurable differences in the vertical water-entry cavity of the hemispherical-head missile. Second, this head shape has the added advantage of relative stability at water entry, which reduces the chance of the density effect being obscured by any fluctuations of the cavitation number or small differences in missile attitude at water entry. The contours of the body and tail sections of the missile were selected for ease in machining. An arbitrary length-to-diameter ratio of six was chosen for the missiles.

Launcher restrictions limited the prototype model to a diameter of 2 inches. Two smaller models, 1-inch and 1/2-inch in diameter, geometrically and dynamically similar to the prototype, were used (Fig. 1). Missile dimensions and parameters are shown in Table 1.

LAUNCHING FACILITIES

The Variable-Angle Variable-Pressure Launching Tank in the NOTS Hydroballistics Laboratory was used in these studies (Ref. 8). In this tank, models up to 2 inches in diameter can be launched at entry velocities as high as 120 ft sec^{-1} . The entry velocities are measured with a photoelectric timer during the air flights of the missiles. The trajectory angle at water entry can be varied from 5 to 90 degrees from the horizontal, and the gas pressure over the water surface can be varied from 1.5 to less than 0.1 atmosphere absolute. Side-view pictures of the missile and of the underwater cavity are taken with a rotating-disk camera illuminated by Edgerton-type flash lamps. Time along the missile trajectory can be determined from the known flash rate of these lamps. A more complete description of these facilities can be found in Ref. 9 and 10.

TEST CONDITIONS

An axially symmetric cavity is formed only if the trajectory and axis of the missile are vertical at water entry. This condition was selected because the simplest entry cavity was desired for the initial study. A test schedule was established to investigate the effect of the following scaling conditions on water-entry cavity modeling:

1. One-to-one Froude number and gas-density scaling
2. One-to-one Froude and cavitation-number scaling
3. One-to-one Froude, cavitation-number and gas-density scaling

This schedule is shown in Table 2. Although the program seems similar to a previous study (Ref. 6), it differed in two significant points. First, water-entry cavity behavior for a missile shape with a hemispherical nose cannot be assumed to be the same as that of a sphere; and second, this program was specifically designed to evaluate scaling techniques, whereas the other study was more general in nature.

Originally it was intended to choose model launching conditions to scale a 4-inch-diameter prototype launched under atmospheric conditions into water at 170 ft sec^{-1} . The choice of such conditions would not limit the model program in the Variable-Angle Variable-Pressure Launching Tank, and should 4-inch-diameter

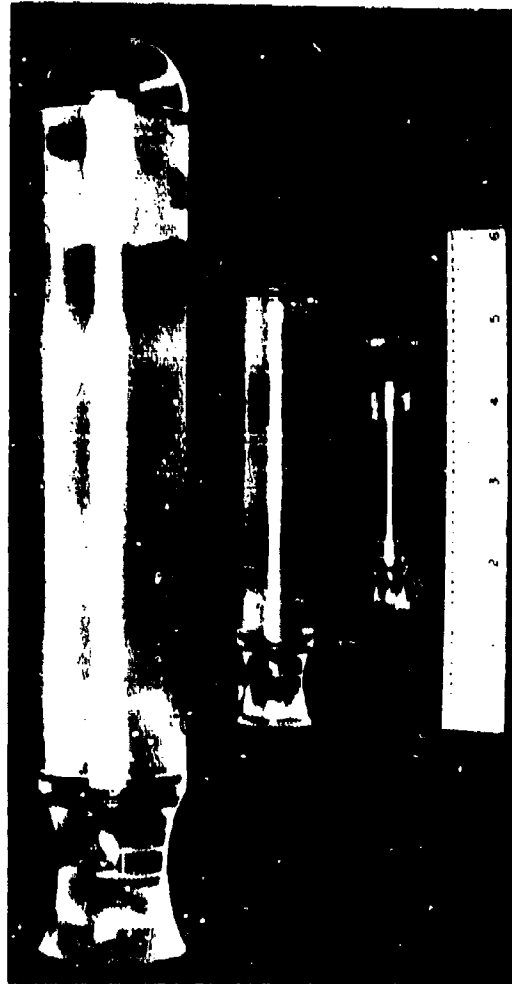
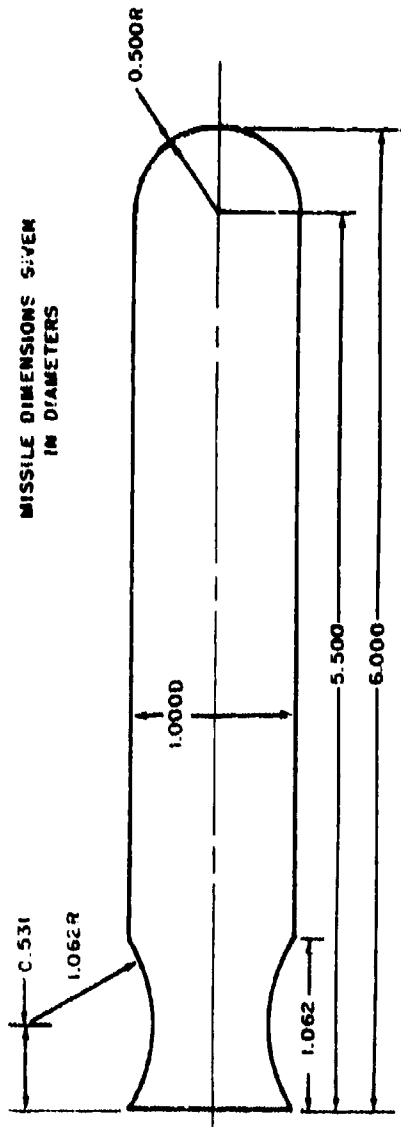


FIG. 1. Missile Configurations.

TABLE 1. Prototype and Model Dimensions

Dimension	2-in.-Diam. Prototype	1-in.-Diam. Model		1/2-in.-Diam. Model	
		Required by Froude Scaling $\lambda = 1/1.999$	Used	Required by Froude Scaling $\lambda = 1/4.012$	Used
Diameter, in.	1.998	0.999	0.999	0.498	0.498
Length, in.	12.016	6.011	6.005	2.995	3.007
Weight, lb	1.128	0.139	0.141	0.017	0.017
Distance of CG From Nose, in.	5.90	2.95	2.92	1.47	1.47
Moment of Inertia ^a , lb in ²	15.61	0.489	0.49	0.015	0.015

^a About a transverse axis through the CG.

TABLE 2. Vertical Water-Entry Modeling Studies With Hemispherical-Head Models

Model		Froude No. Scaled, F = 51.8 Cavitation No. Not Scaled Gas Density Coeff. Scaled, $\rho' = 0.8$				Froude No. Scaled, F = 51.8 Cavitation No. Scaled, $\sigma = 0.073$ Gas Density Coeff. Not Scaled				Froude No. Scaled, F = 51.8 Cavitation No. Not Scaled Gas Density Coeff. Scaled, $\rho' = 0.8$				Froude No. Scaled, F = 51.8 Cavitation No. Not Scaled Gas Density Coeff. Scaled, $\rho' = 1.0$			
		Gas Pres- sure, atm	Gas Den- sity Coeff.	Gases Used	Gas Pres- sure, atm	Gas Den- sity Coeff.	Gases Used	Gas Pres- sure, atm	Gas Den- sity Coeff.	Gases Used	Gas Pres- sure, atm	Gas Den- sity Coeff.	Gases Used	Gas Pres- sure, atm	Gas Den- sity Coeff.		
Di- ameter, in.	Ve- locity, ft sec ⁻¹	2	1	0.8	A+He	1/2	0.4	A+He	1/2	0.8	A+F12	1	1.0	A			
		1	1	0.8	A+He	1/4	0.2	A+He	1/4	0.8	A+F12	1	1.0	A			
		1/2	1	0.8	A+He	1/8	0.1	A+He	1/8	0.8	F114B2	1	1.0	A			

NOTES:

Triplicate launchings made for each water-entry condition.

One atmosphere pressure is taken to be 740-mm Hg (ambient at laboratory and Morris Dam).

A = air, He = helium, F12 = Freon 12 (dichlorodifluoromethane).

F114B2 = Freon 114B2 (dibromotetrafluoroethane).

prototype launchings become feasible at a later date, the modeling scale ratio could be extended by inclusion of these prototype launchings.

In describing gas pressures and densities, it was found convenient to define reference standards. Since average ambient conditions of temperature and pressure at the Morris Dam Torpedo Range (where prototype tests were contemplated) and the Hydroballistics Laboratory at NOTS approximated 20°C and 740 mm of mercury, it was convenient to define 1 atmosphere as 740 mm of mercury. Gas densities are described in terms of a gas-density coefficient ρ' , which is the ratio of the density of the gas (irrespective of its associated conditions of temperature and pressure) to that of air at 20°C and 740-mm pressure.

The desired gas densities were obtained by mixing air with two heavy gases, Freon 12 (dichlorodifluoromethane, Ref. 11) and Freon 114B2 (dibromotetrafluoroethane, Ref. 12), which have densities, respectively, four and nine times greater than air, under the same conditions of temperature and pressure. Theoretically, it should be possible to obtain a gas-density coefficient of 1 over a water surface with a gas nine times as heavy as air at a pressure of 1/8 atmosphere if the water-vapor pressure is not greater than 10 mm of mercury. For this reason the tank water was chilled to 10°C, thereby reducing the vapor pressure to 9 mm of mercury. However, the tank leaked air causing the maximum gas-density coefficient obtainable at 1/8 atmosphere to be 0.8. Therefore it was decided to take a gas-density coefficient of 0.8 as the "reference" atmospheric density, even though this meant the impossibility of future one-to-one gas-density scaled tests with the 4-inch-diameter model. Helium was added to air to reduce its gas-density coefficient to 0.8 for the full atmospheric pressure launchings. Model launchings were also made at atmospheric pressure and a gas-density coefficient of 1.0. This was done to determine to what extent prototype cavities having a gas-density coefficient of 1.0 could be predicted from a modeling system having a gas-density coefficient of 0.8.

The Variable-Angle Variable-Pressure Launching Tank was evacuated until the calculated amount of air and water vapor, as determined by pressure, remained. Freon or Helium was then added to bring the gas mixture simultaneously to the desired launching density and pressure. The gases were mixed by a small fan in the dome of the tank. Immediately before launching, the fan was stopped and a gas sample withdrawn from a point approximately 6 inches above the water surface. The sample, taken at tank pressure, was drawn into a calibrated gas-density balloon and the gas density determined gravimetrically.

In order to determine if the presence of varying amounts of air in the water altered the entry cavity, several launchings were made into water having different air contents¹. It was found that although the size and shape of the cavity were unaltered by the presence of excess air, the texture of the cavity wall became rough when the air content exceeded the equilibrium concentration with air at atmospheric pressure. Since well-defined cavity contours were desired, this equilibrium concentration was carefully maintained during all tests.

The launching conditions are shown in Table 3. Triplicate launchings were made under each test condition.

The 2-inch-diameter prototype was tracked at least 25 diameters after water entry, the 1-inch-diameter model for 35 diameters, and the 1/2-inch-diameter model for 45 diameters. The prototype model was photographed at 0.0025-second time intervals. The smaller models were photographed at shorter time intervals of 0.00167 and 0.00125 second, respectively, which scale approximately as $\sqrt{\lambda}$. Zero time was defined as the instant of contact between the missile and the water surface. The accuracies with which the entry conditions of the model and the characteristics of the cavity could be measured are listed in Table 4.

DISCUSSION OF RESULTS

Figure 2 reproduces a typical film from the rotating-disk camera, which illustrates the water-entry of the 1-inch-diameter model launched with a water-contact velocity of approximately 85 ft sec⁻¹ and in an atmospheric mixture of air and Freon 12. The gas pressure was 1/4 atmosphere and the gas density coefficient 0.8. To preclude any ambiguity in the terms "surface closure" and "deep closure," the cavity closures are indicated in Fig. 2.

¹ The photographs taken to investigate the effects of water air-content revealed two interesting aspects of cavity flow that were not directly related to water-entry cavity modeling. First, because the transient water-entry cavities were sufficiently similar to steady-state cavities observed in water tunnels, a separate study was made to assess the feasibility of predicting water-entry cavity pressures from the known pressures in steady-state cavities. Second, transverse circular striae that could have been caused by longitudinal vibration of the missile at water impact were observed on water-entry cavity walls. These aspects of cavity flow are discussed in Appendixes A and B.

TABLE 3. Missile Launching Conditions

NAVORD REPORT 5365, Part I

Nominal entry angles: trajectory = 90 deg. angle of attack = 0 deg; water temperature: $10 \pm 2^\circ\text{C}$; gas temperature: $18 \pm 3^\circ\text{C}$.

Modeling Condition	Prototype, 2-in. Diam.				Model, 1-in. Diam.				Model, 1/2-in. Diam.			
	ML No.	Entry Velocity, ft sec ⁻¹	Gas Pressure, Std. atm ^a	Gas Density Coef.	ML No.	Entry Velocity, ft sec ⁻¹	Gas Pressure, Std. atm ^a	Gas Density Coef.	ML No.	Entry Velocity, ft sec ⁻¹	Gas Pressure, Std. atm ^a	Gas Density Coef.
Froude no. scaled, $F=51.8$. . .	1662	119.9	1.00	0.80	1637	87.3	1.00	0.78	1629	60.7	1.00	0.79
Cavitation no. not scaled	1663	120.2	1.00	0.79	1638	87.6	1.00	0.78	1630	60.2	1.00	0.78
Gas-density coef. scaled, $p'=0.8$. . .	1664	120.3	1.00	0.78	1639	84.5	1.00	0.79	1631	60.1	1.00	0.78
Froude no. scaled, $F=51.8$. . .	1659	120.6	0.50	0.40	1646	83.2	0.25	0.21	1672	61.5	0.12	0.11
Cavitation no. scaled, $\sigma=0.073$. .	1660	120.6	0.50	0.39	1648	88.8	0.25	0.22	1674	61.4	0.12	0.09
Gas-density coef. not scaled	1661	120.6	0.50	0.41	1669	85.9	0.25	0.20	1676	62.8	0.12	0.09
Froude no. scaled, $F=51.8$. . .	1655	120.6	0.50	0.81	1651	81.8	0.25	0.85	1624	59.9	0.12	0.79
Cavitation no. scaled, $\sigma=0.073$. . .	1656	120.5	0.50	0.79	1652	80.2	0.25	0.85	1626	61.9	0.12	0.88
Gas-density coef. scaled, $p'=0.8$. . .	1657	120.6	0.50	0.83	1667	83.2	0.25	0.81	1627	61.9	0.12	0.85

Froude no. scaled, $F=51.8$. .	1598	118.8	1.00	1(nom)	1633	85.0	1.00	1.01	1605	63.6	1.00	1.01
Cavitation no. not scaled	1603	120.9	1.00	1.00	1634	87.2	1.00	1.01	1607	62.6	1.00	1.00
Gas density coef. scaled, $\rho'=1.0$. .	1604	118.1	1.00	1.00	1635	83.5	1.00	1.01	1617	59.5	1.00	1(nom)

^a Standard atmosphere taken as 740 mm of Hg pressure.

TABLE 4. Accuracy of Measurement of Entry Conditions and Cavity Characteristics

Quantity Measured	Accuracy of Measurement Prototype Scale
Ambient Conditions	
Water temperature	$\pm 1/4^{\circ}\text{C}$
Gas temperature	$\pm 1/4^{\circ}\text{C}$
Gas density	$\pm 0.005 \rho'$
Gas pressure	$\pm 0.005 \text{ atm}$
Entry Velocity of Missiles	
2-in. diam. prototype	$\pm 1/2 \text{ ft sec}^{-1}$
1- and 1/2-in. diam. models	$\pm 3 \text{ ft sec}^{-1}$
Time	
Flash rate of lights cycles/sec.	$\pm 1 \mu\text{s}$
Zero time	$\pm 1.5 \text{ ms}$
Cavity Characteristics	
Closures	
2-in. diam. prototype	$\pm 1.3 \text{ ms}$
1- and 1/2-in. diam. models	$\pm 1.2 \text{ ms}$
Diameter	$\pm 1/8 \text{ in.}$
Area	$\pm 5 \text{ in}^2$

Surface closure is defined as the closure of the water surface itself and not the dome of the splash, and deep closure is defined as any permanent break in the cavity beneath the water surface. The photographs of the missiles were measured to determine the growth and closure of the entry cavities. Parameters measured and plotted as functions of time were: (1) the time and position of cavity closures, (2) the cavity diameter at the missile tail, and (3) the projected cavity area in a vertical plane containing the cavity axis of symmetry. In order to make the curves describing the cavity behavior of the three missiles directly comparable, the model data were scaled to prototype size by multiplying distances by $1/\lambda$, areas by $1/\lambda^2$, and time by $1/\sqrt{\lambda}$. These data are shown in Fig. 3-5. Closure, diameter, and area curves from each test condition are presented in the same illustration to provide a better insight into cavity behavior. The area bracketed by the data from each set of three duplicate curves was presented instead of an average curve in order to show both the behavior of the cavity and its reproducibility. When the cavity behavior was erratic, the three individual curves were plotted separately.

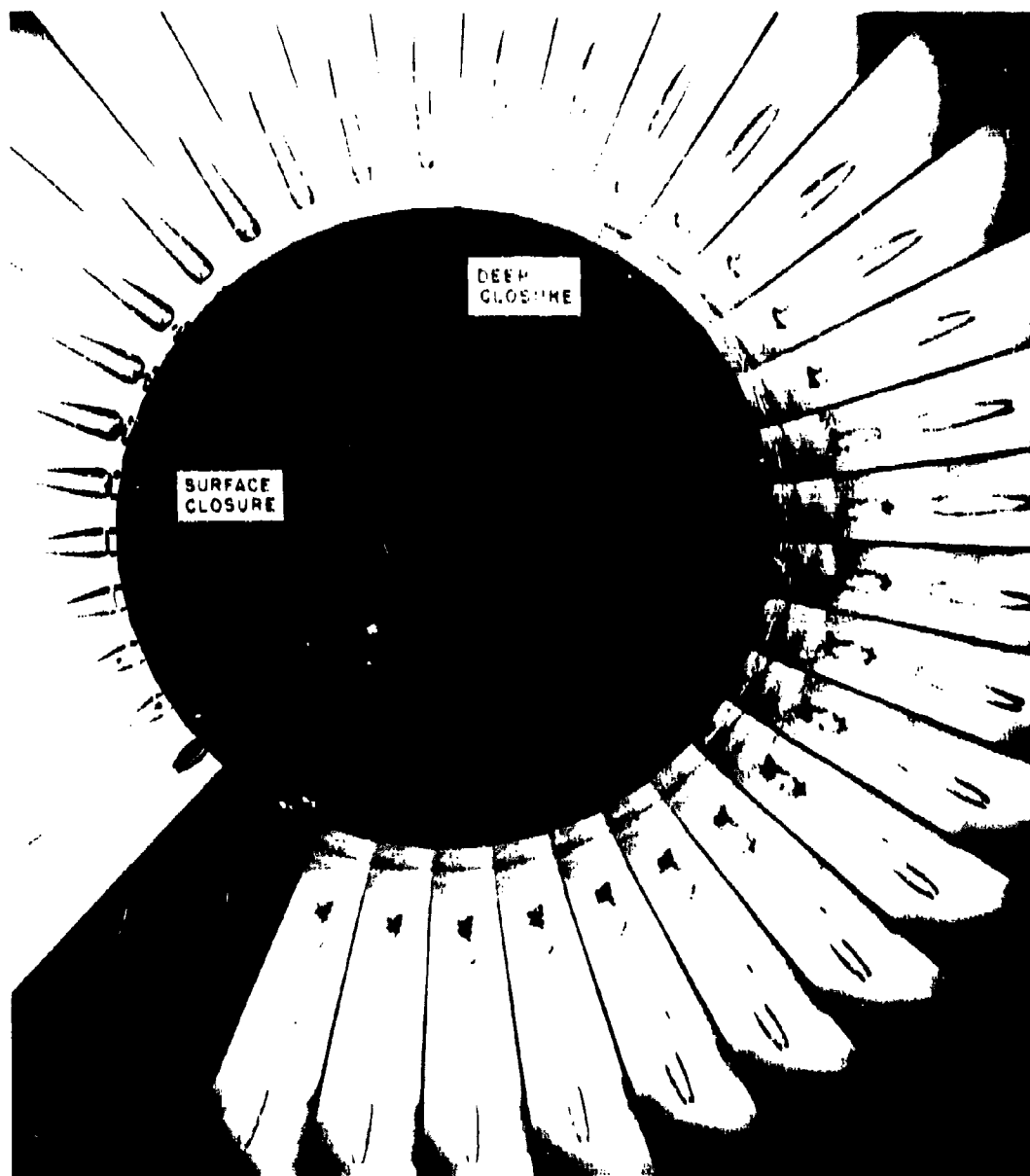


Figure 1. A. Surface closure. B. Deep closure.

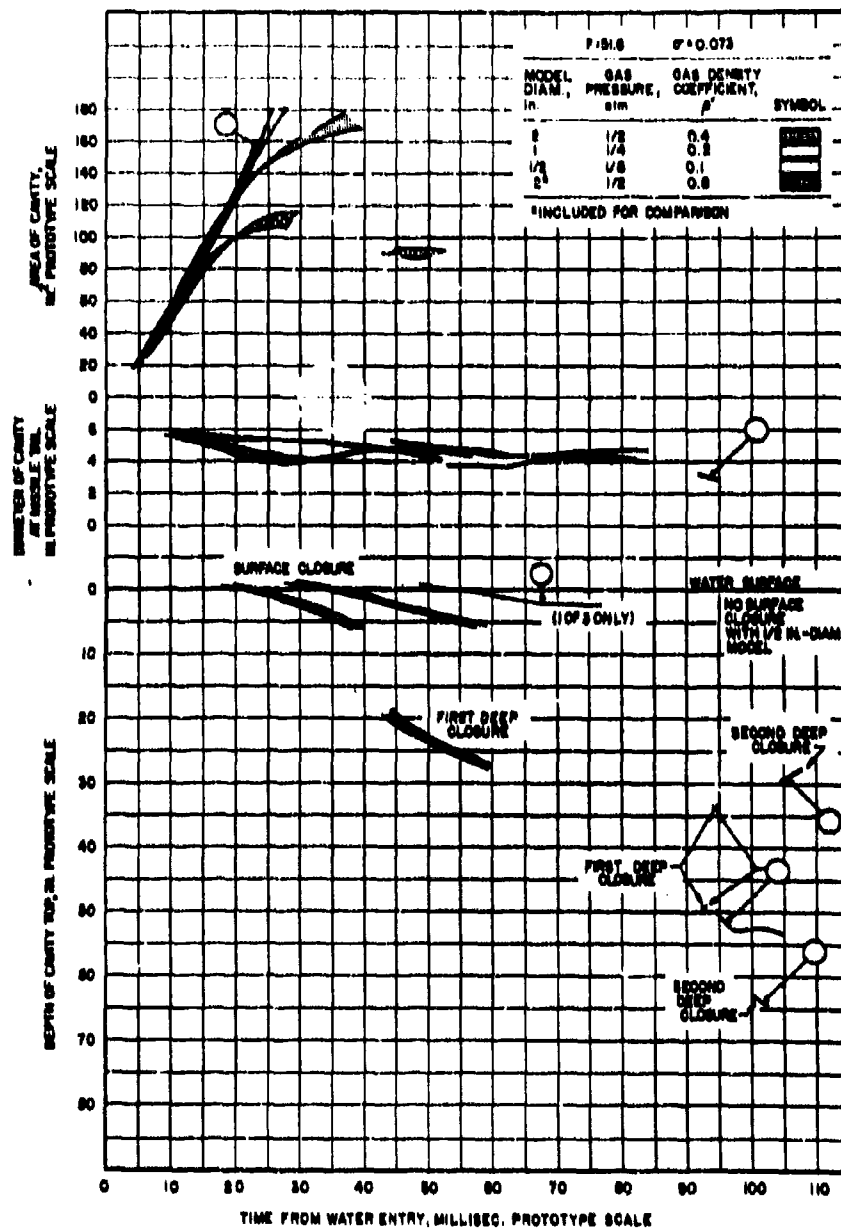


FIG. 3. Comparisons of Cavity Parameters With One-to-One Froude- and Cavitation-Number Scaling.

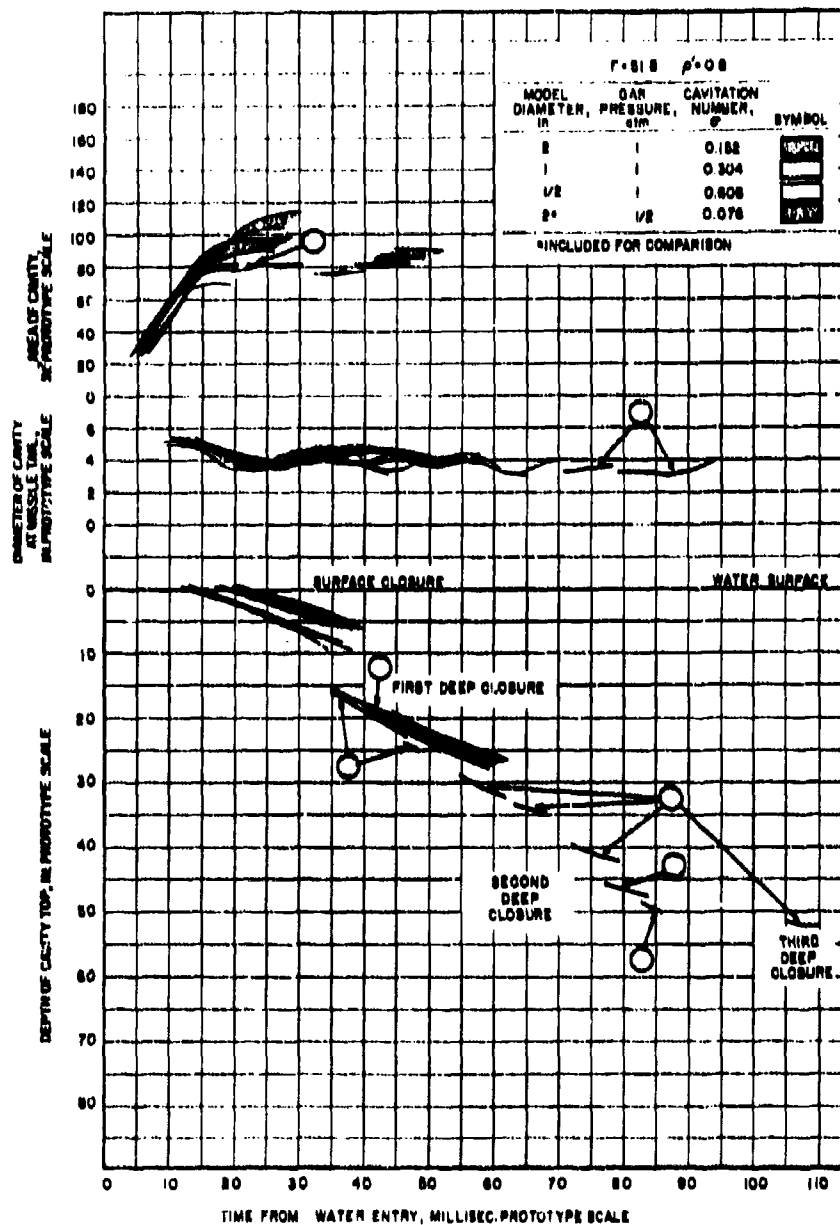


FIG. 4. Comparison of Cavity Parameters With One-to-One Froude-Number and Gas-Density Scaling.

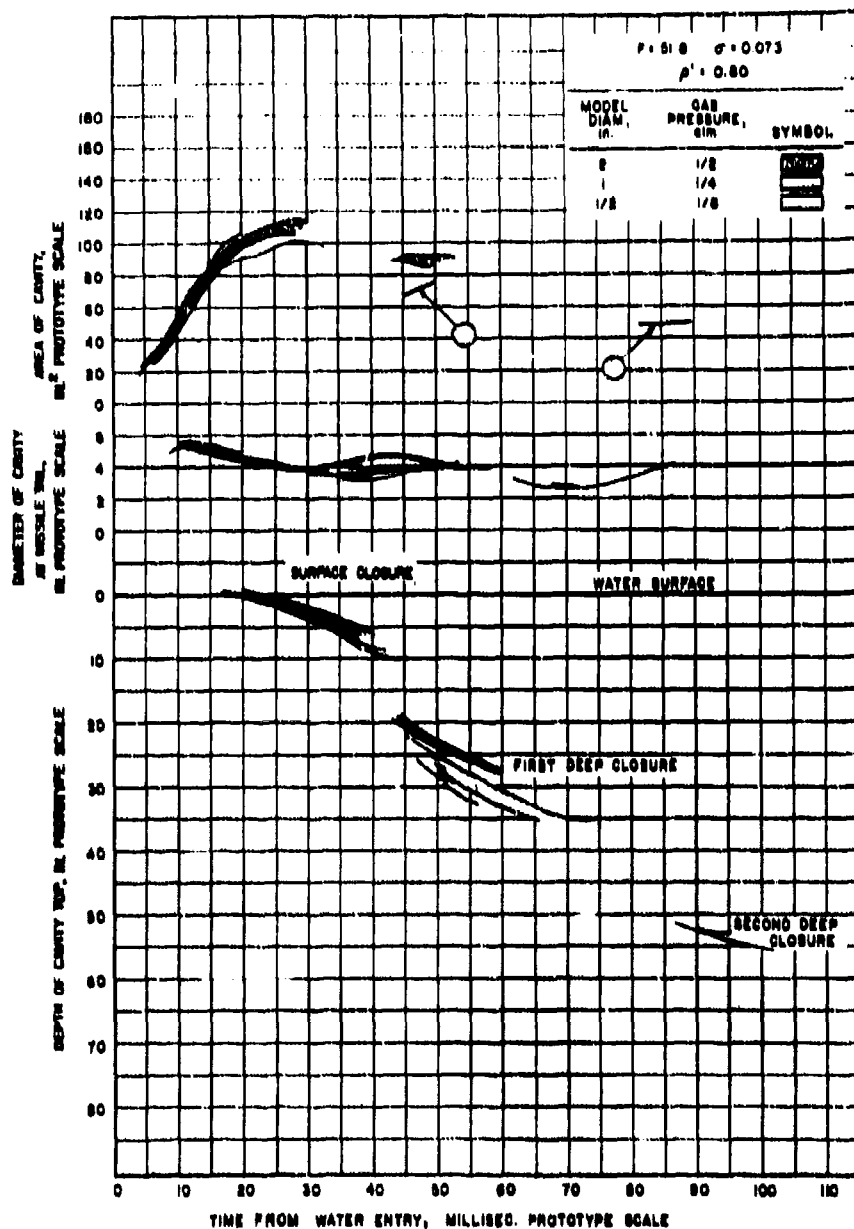


FIG. 5. Comparison of Cavity Parameters With One-to-One Froude- and Cavitation-Number and Gas-Density Scaling.

CAVITY CLOSURE

The three missiles formed reproducible cavities under the same entry conditions as long as a gas-density coefficient of 0.8 or higher was maintained. These cavities always closed first at the water surface. When the gas-density coefficient was allowed to decrease with the atmospheric pressure, cavity closure became erratic under supposedly equal entry conditions. Surface closure was late, and in some instances followed deep closure or failed to occur during the recorded trajectories. The cavity closures are extremely important in determining cavity history because (1) the mass of gas in the cavity cannot appreciably increase after the water surface closes, and (2) the persistence of the cavity about the missile is largely determined by the time and place of deep closure.

Both surface and deep closure always occurred in such a fashion that the newly formed seal at the top of the cavity was flat and essentially parallel to the water surface. The depth of the cavity top was measured and plotted as a function of time after water entry. A separate curve resulted from each seal. The earliest point on each curve was located at the time and depth at which the seal occurred, and subsequent points marked the later positions of the top of the cavity remaining about the missile. In many instances several deep closures occurred during a single launching. Depth measurements were terminated when the flat surfaces were no longer sufficiently well defined to be measured accurately.

Figures 3-5 compare the closures obtained with one-to-one Froude and cavitation-number or Froude-number and gas-density scaling to those obtained with Froude and cavitation number and gas density scaled simultaneously. Neither surface nor deep closure was modeled unless the condition of one-to-one gas-density scaling was included. Then both closures were scaled to a good degree of accuracy with or without one-to-one scaling of cavitation number, although modeling of surface closure was slightly improved by scaling cavitation number. No numerical comparison could be made with the data presented in Ref. 6. However, a generally similar pattern of cavity closure was observed during both investigations.

The ratio of the difference in depth to the difference in time between surface and first deep closure (Fig. 3-5) provides an index of cavity modeling. If the ratio for the 2-inch-diameter missile with one-to-one Froude and cavitation-number and gas-density scaling is taken as the prototype modeling condition, a closure parameter ω which compares cavity-closure modeling under the different scaling conditions can be defined as follows:

$$(15) \quad \omega = \left(\frac{\lambda^{-1} \Delta h}{\lambda^{-1/2} \Delta t} \right) / \left(\frac{\Delta h_p}{\Delta t_p} \right)_* = \left(\frac{\lambda^{-1/2} \Delta h}{\Delta t} \right) / \left(\frac{\Delta h_p}{\Delta t_p} \right)_*$$

where Δh is the difference in depth and Δt is the difference in time between surface and first deep closure. Depth and time in the numerator of Eq. 15 have been scaled to prototype conditions, and the denominator $(\Delta h_p / \Delta t_p)_*$ represents the ratio for the prototype modeling condition. Subscripts are not used in the numerator because ratios for both prototype and models are used. For perfect cavity closure modeling, $\omega = 1$. As modeling fails, ω deviates progressively from this value. From Fig. 6 where ω is plotted as a function of gas pressure and scaling conditions, it is evident that one-to-one gas-density scaling is necessary for modeling the closure parameter and that one-to-one cavitation-number scaling is of relatively little importance.

CAVITY DIAMETER

For convenience, the cavity diameter curves from Fig. 3-5 are reproduced together in Fig. 7. The magnitude of the cavity diameter at the missile tail, which was measured only when the tail was not in contact with the cavity wall, was not much altered by the various scaling techniques employed. Under no circumstances did these curves deviate more than one missile diameter from the prototype condition. However, marked oscillations appeared in the diameter-time curves that were obviously not modeled by any scaling technique used in this investigation. It was observed that:

1. Oscillation occurred only after the cavity was closed from the atmosphere above the water surface.
2. The period of the oscillation increased with
 - (a) increase in missile diameter at constant Froude number,
 - (b) decrease in gas density, and
 - (c) decrease in gas pressure.

The periods of the oscillation, T , were sufficiently well defined in several instances to be measurable and were found to be expressible as $T(p')^4/d^4 = 0.024$ second prototype time at $F = 51.8$, $p' = 0.8$ or 1.0 , and $p_g = 1$ atmosphere. Although this relationship admittedly is based upon few data, and may be no more than a fortuitous coincidence, it may serve as a guide in further investigation of this cavity oscillation.

CAVITY VOLUME FROM PROJECTED CAVITY AREA

The projected cavity area provides an index for comparison of cavity volume when the cavities are geometrically similar. For geometrically similar cavities

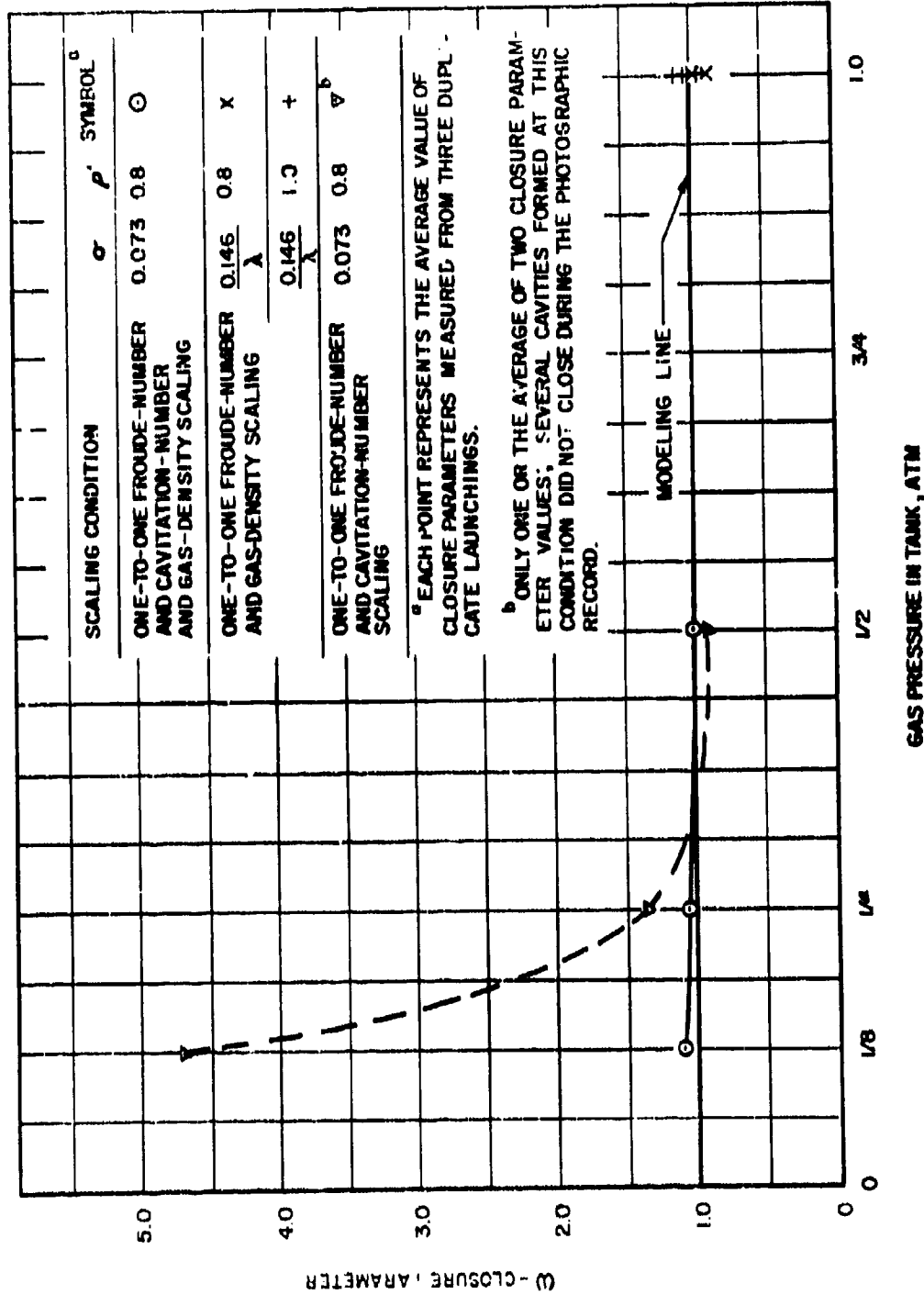


FIG. 6. Closure Parameter as a Function of Gas Pressure and Scaling Condition.

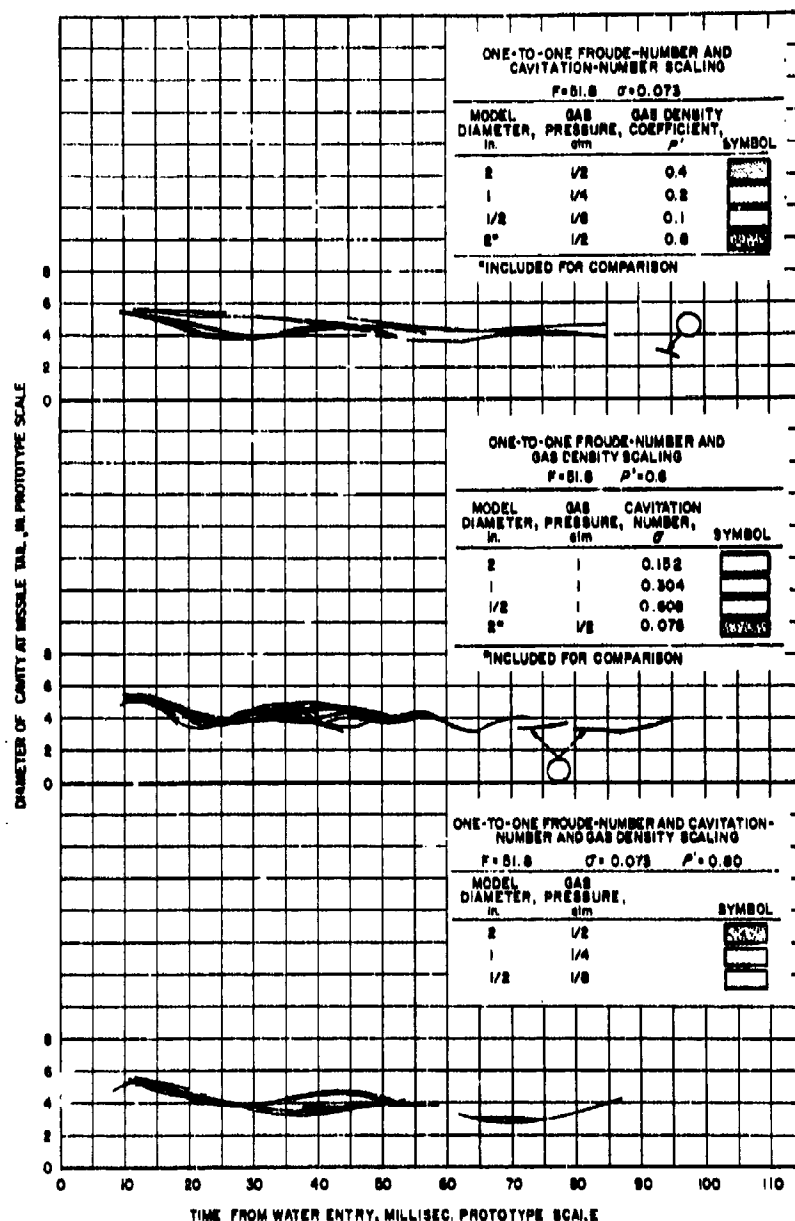


FIG. 7. Variation in Cavity Diameter With Model Size and Scaling Conditions.

(16) Ratio of cavity volumes = λ ratio of projected cavity areas

The shape of the cavity was distorted when the missile tail struck the cavity wall and area measurements were terminated at first tail contact. When the cavity was broken by deep closure, the area of the cavity remaining about the missile was measured.

When the atmospheric density was 0.8 or higher, the shapes of the cavities made by the three missiles were sufficiently similar throughout the trajectory that cavity area could be considered proportional to cavity volume (Fig. 8). Figure 9 shows that fair modeling of cavity volume was achieved by one-to-one scaling of Froude and gas density, and that excellent modeling resulted when the cavitation number was also scaled. Successful modeling of cavity volumes, with 1-inch and 1/2-inch-diameter spheres in a one-to-one Froude and cavitation-number and gas-density scaled system, was also reported in Ref. 6.

When gas density was not scaled, the cavities from the three missiles were initially similar. Later in the trajectory, however, they became quite different in shape (Fig. 10), and no direct comparison of volume could be made. However, both the photographs and the area curves indicate that the cavity became excessively large as the model diameter, and hence the atmospheric density, decreased.

It is felt that the cavity-area curves substantiate the definition of surface closure employed throughout these tests since the cavities ceased to increase in size about the time of surface closure (Fig. 3-5).

MISSILE MOTION IN UNDERWATER CAVITY

From Eq. 1, 8, and 9, missile water penetration distance will be modeled if the distance, expressed in diameters, is the same when the corresponding times of penetration scale as $\sqrt{\lambda}$. Measurements of missile penetration distances for scaled times of penetration were made and distances corresponding to 0.05 second prototype scale are shown in Table 5. These data represent the greatest distance for which modeling comparison could be made. The data indicate that good water penetration distance modeling was obtained for all modeling conditions used. Furthermore, there is no evidence that the penetration distance was affected by the modeling condition.

From Eq. 11, 12, 13, and 14, missile orientation will be modeled if the orientation is the same when the times of penetration scale as $\sqrt{\lambda}$. However, launcher vibration gave the models varying angular velocities in air flight with the result that missile water-entry










SCALING CONDITION	2-IN.-DIAM. PROTOTYPE	1-IN.-DIAM. MODEL	1/2-IN.-DIAM. MODEL
$F = 51.8$ $\rho^* = 0.8$ σ^* CAVITY LENGTH SCALED TO PROTOTYPE DIMENSIONS L/D_{max}	 $\sigma^* = 0.146$ $L/D_{max} = 1.50$ $L/D_{max} = 3.13$	 $\sigma^* = 0.292$ $L/D_{max} = 1.44$ $L/D_{max} = 3.18$	 $\sigma^* = 0.584$ $L/D_{max} = 1.36$ $L/D_{max} = 3.18$
$F = 51.8$ $\rho^* = 1.0$ σ^* CAVITY LENGTH SCALED TO PROTOTYPE DIMENSIONS L/D_{max}	 $\sigma^* = 0.146$ $L/D_{max} = 1.41$ $L/D_{max} = 3.18$	 $\sigma^* = 0.292$ $L/D_{max} = 1.32$ $L/D_{max} = 3.08$	 $\sigma^* = 0.584$ $L/D_{max} = 1.44$ $L/D_{max} = 3.29$
$F = 51.8$ $\sigma^* = 0.073$ $\rho^* = 0.8$ CAVITY LENGTH SCALED TO PROTOTYPE DIMENSIONS L/D_{max}	 $L/D_{max} = 1.48$ $L/D_{max} = 3.08$	 $L/D_{max} = 1.48$ $L/D_{max} = 3.03$	 $L/D_{max} = 1.44$ $L/D_{max} = 3.14$

FIG. 8. Shape of the Vertical Water-Entry Cavity. One-to-one Froude-number and gas-density scaling with and without one-to-one cavitation-number scaling.

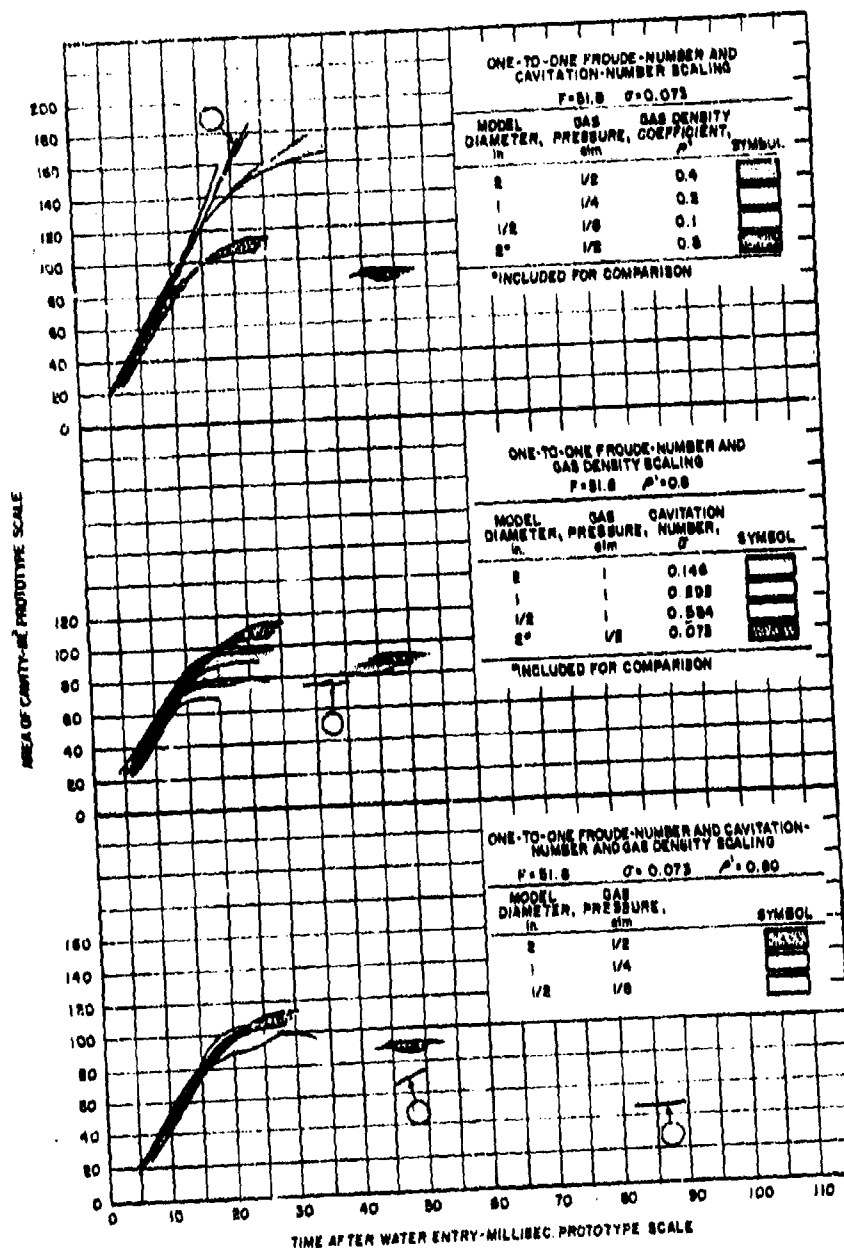


FIG. 9. Variation of Projected Cavity Area With Model Size and Scaling Conditions. (Summary of time-volume curves of Fig. 3-5).







SCALING CONDITION	2-IN.-DIAM. PROTOTYPE	1-IN.-DIAM. MODEL	1/2-IN.-DIAM. MODEL
$F = 51.8$ $\sigma = 0.078$			
ρ^1 CAVITY LENGTH SCALED TO PROTOTYPE DIMENSIONS L/D_{max}	0.4 1.37 2.61	0.2 1.48 2.78	0.1 1.60 2.78
$F = 51.8$ $\sigma = 0.073$			
ρ^1 CAVITY LENGTH SCALED TO PROTOTYPE DIMENSIONS L/D_{max}	0.4 36.7 8.64	0.2 40.8 4.84	0.1 38.4 2.78

FIG. 10. Shape of the Vertical Water-Entry Cavity. One-to-one Froude-number and cavitation-number scaling.

orientation and angular velocity varied from launching to launching. Therefore it was not possible to study the modeling of missile orientation in the cavity.

TABLE 5. Penetration Distance in Diameters

Penetration distance measured to nose of missile at 0.05 second after water entry, prototype scale.

Modeling Condition	Prototype, 2-inch Diam.		Model, 1-inch Diam.		Model, 1/2-inch Diam.	
	ML No.	Distance, Diam.	ML No.	Distance, Diam.	ML No.	Distance, Diam.
F = 51.8 σ not scaled $\rho' = 0.8$	1662	23.5	1637	23.5	1629	24.3
	1663	23.6	1638	23.6	1630	23.8
	1664	23.8	1639	23.3	1631	23.8
F = 51.8 $\sigma = 0.073$ ρ' not scaled	1659	23.7	1646	23.2	1672	24.4
	1660	24.6	1648	23.4	1674	25.1
	1661	23.8	1669	23.8	1676	21.6 ^a
F = 51.8 $\sigma = 0.073$ $\rho' = 0.8$	1655	23.0	1651	23.0	1624	23.5
	1656	23.5	1652	22.7	1626	24.3
	1657	24.6	1667	23.0	1627	23.8
F = 51.8 σ not scaled $\rho' = 0.8$	1598	23.7	1633	23.2	1605	24.4
	1603	24.0	1634	23.8	1607	24.5
	1604	23.9	1635	23.5	1617	24.5

^a Extreme yaw and tail contact at water entry.

SCALING OF FULL-SIZE MISSILES

Predicting the water-entry and underwater-trajectory behavior of a full-size (22.4-inch diameter) missile from a 2-inch-diameter model involves a scale factor $\lambda = 1/11$. One-to-one Froude- and cavitation-number and gas-density scaling would require that the gas pressure be reduced to 1/11 atmosphere, while the gas-density coefficient be kept equal to 1.0. At this pressure the heaviest gas presently available which is suitable for modeling studies (dibromotetrafluoroethane), when saturated with water vapor at ambient temperature, has a density coefficient of 0.74. Therefore the difference in behavior produced by increasing the gas-density coefficient from 0.8 to 1.0 is of interest. In Fig. 11-13 results from tests made with one-to-one Froude-number and gas-density

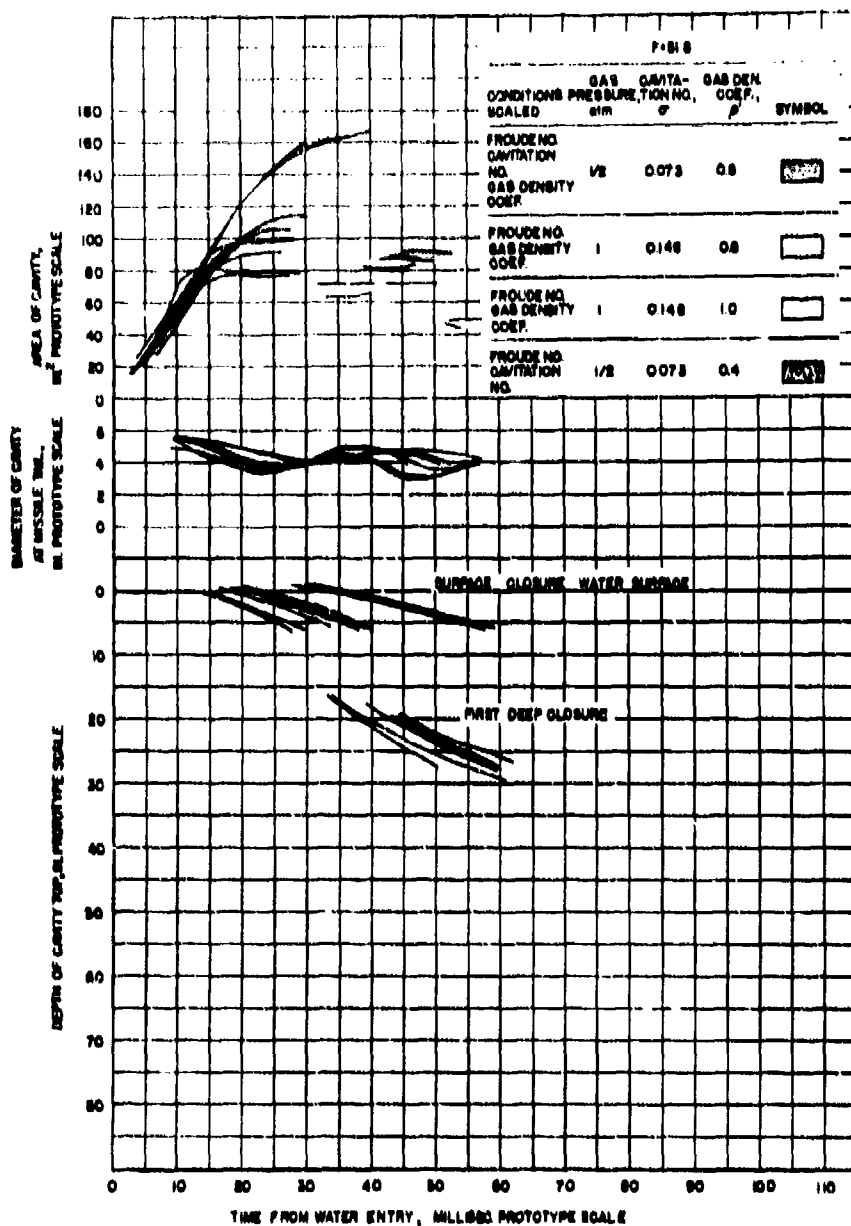


FIG. 11. Effect of Scaling Conditions on Cavity Parameters of 2-Inch-Diameter Model.

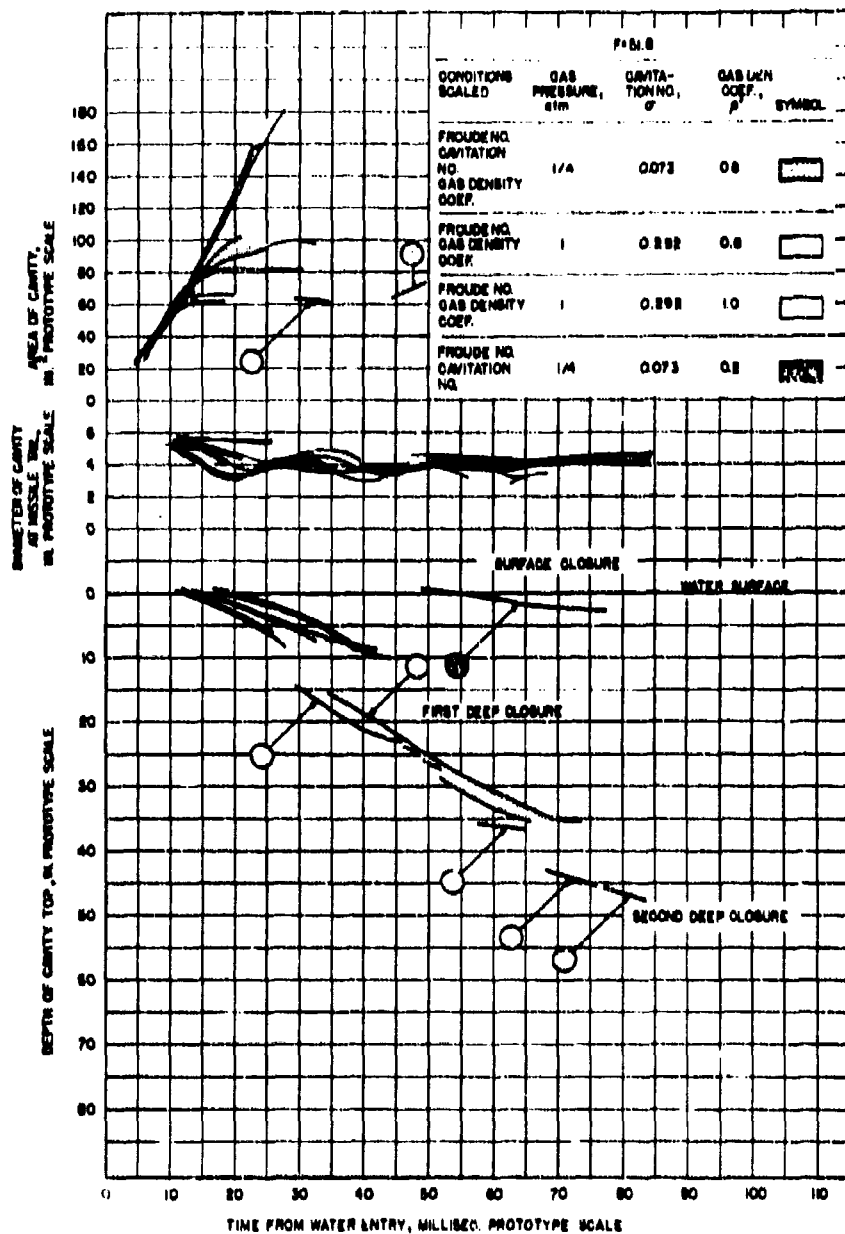


FIG. 12. Effect of Scaling Conditions on Cavity Parameters of 1-Inch-Diameter Model.

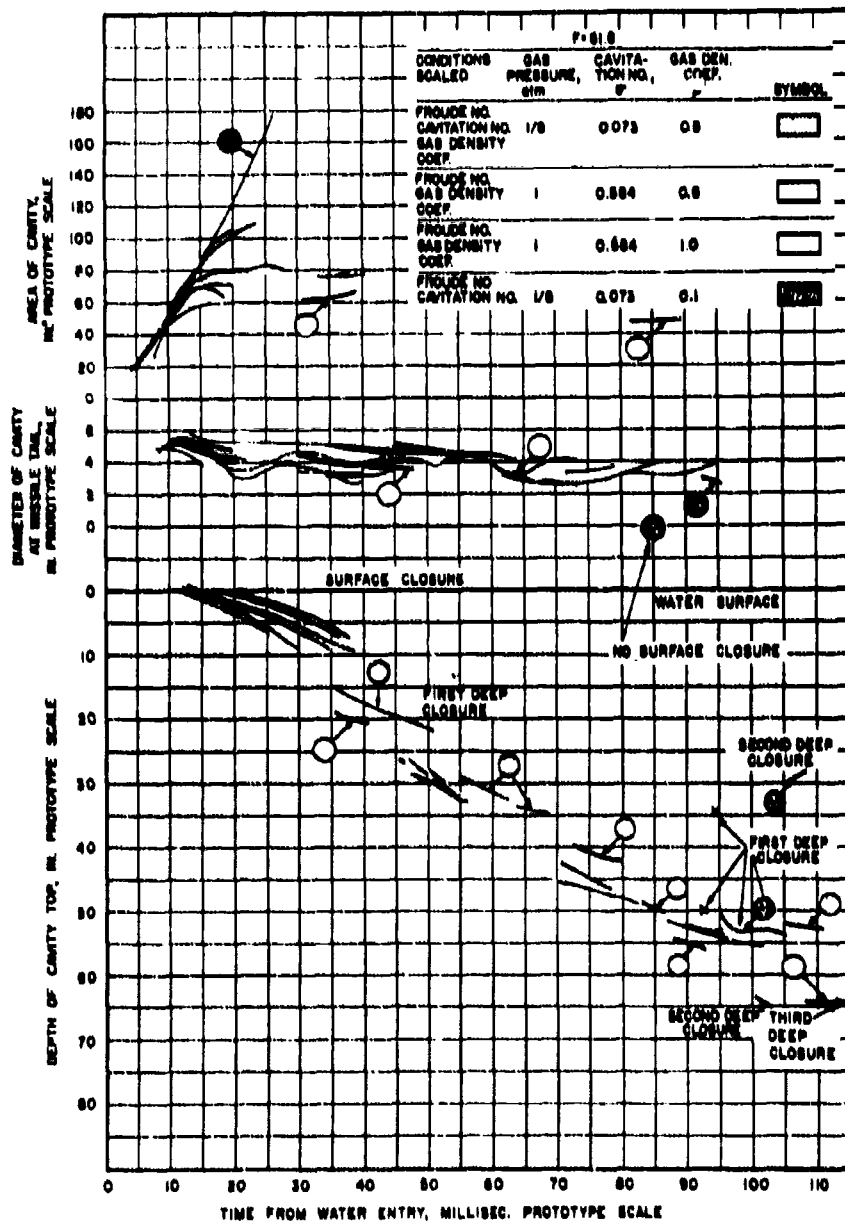


FIG. 13. Effect of Sealing Conditions on Cavity Parameters of 1/2-Inch-Diameter Model.

scaling (gas-density coefficient equal to 1.0) are compared with the data from Fig. 3-5. For convenience and clarity, behavior of each of the three missiles is plotted separately. The change in cavity behavior as a result of variation in atmospheric density from 0.8 to 1.0 was small compared to the large change caused by complete disregard of gas-density scaling.

Although it might be surmised from these data that full-scale cavity prediction would be much improved by using one-to-one gas-density scaling or approximating this scaling as closely as possible in the model system, it should be noted that full-scale missiles are ordinarily launched at oblique water-entry angles. Hence, the evaluation of the importance of gas-density scaling in modeling service-missile cavities should be deferred to Part 2 of this report, which deals with oblique water entry.

CONCLUSIONS

The following conclusions were drawn from observation of the vertical-entry cavities formed by 2-inch-, 1-inch-, and 1/2-inch-diameter hemispherical-head missiles, scaled in accordance with the Froude law to be geometrically and dynamically similar:

1. One-to-one scaling of Froude and cavitation number and gas density produced excellent modeling of the entry cavities during this series of tests.
2. Rather good agreement among the cavities was also obtained with one-to-one scaling of Froude number and gas density in absence of scaling of cavitation number.
3. One-to-one Froude- and cavitation-number scaling did not model the water-entry cavity. The cavities became excessively large and cavity closure occurred later and became more erratic as the model size was decreased.
4. Good water penetration distance modeling was obtained for all modeling conditions studied. The penetration distance was not affected by the modeling condition.
5. It should not be concluded from these tests that one-to-one scaling of cavitation number need not be observed in modeling the water-entry cavity because cavitation number may prove more important in scaling cavities formed by missiles of other shapes. Furthermore, modeling of missile motion during oblique water entry requires that cavitation number be scaled (Ref. 1-3).

Appendix A

PREDICTION OF CAVITY PRESSURE FROM CAVITY SHAPE

An attempt was made to predict the internal pressure of a transient cavity formed by an air-to-water missile from the known internal pressure of a steady-state cavity formed by the same missile in a water tunnel. A survey of the data from the Variable-Angle Variable-Pressure Tank and the Free Surface Water Tunnel at the California Institute of Technology² indicated that tunnel tests with disks of various sizes oriented at zero angle of attack and tank tests of a disk-cylinder missile ($l/d = 6$) (Fig. 14) launched with vertical trajectory and zero angle of attack would be most suitable for comparison. It was felt that the transient and steady-state cavities should be congruent at least for several diameters along the missile body if any prediction of pressure were to be made.

Cavities from disks 1/2, 3/4, and 1 inch in diameter and with cavitation number, σ , ranging from 0.03 to 0.17 were observed in the water tunnel. The staff of the Free Surface Water Tunnel measured numerous cavity contours and were able to describe them all in terms of the following empirical relationship:

$$(17) \quad \left(\frac{y - y_0}{b_0} \right)^{1.8} + \left(\frac{a_0 - x}{a_0} \right)^2 = 1; \quad 0.03 \leq \sigma \leq 0.17$$

where σ is the cavitation number and a_0 and b_0 , the half-length and half-diameter, are defined in Fig. 15. One quadrant of the curve, which resembles an ellipse, describes the cavity contour between the separation point and the maximum cavity diameter.

The contours of three transient cavities were measured for comparison with Eq. 17. The conditions under which these cavities were formed are listed in Table 6.

Fitting the transient data to Eq. 17 posed a problem because the transient cavity contour was slightly scalloped in appearance as if it were formed by segments from several different cavities.

² Unpublished data from Hydrodynamics Laboratory, California Institute of Technology.

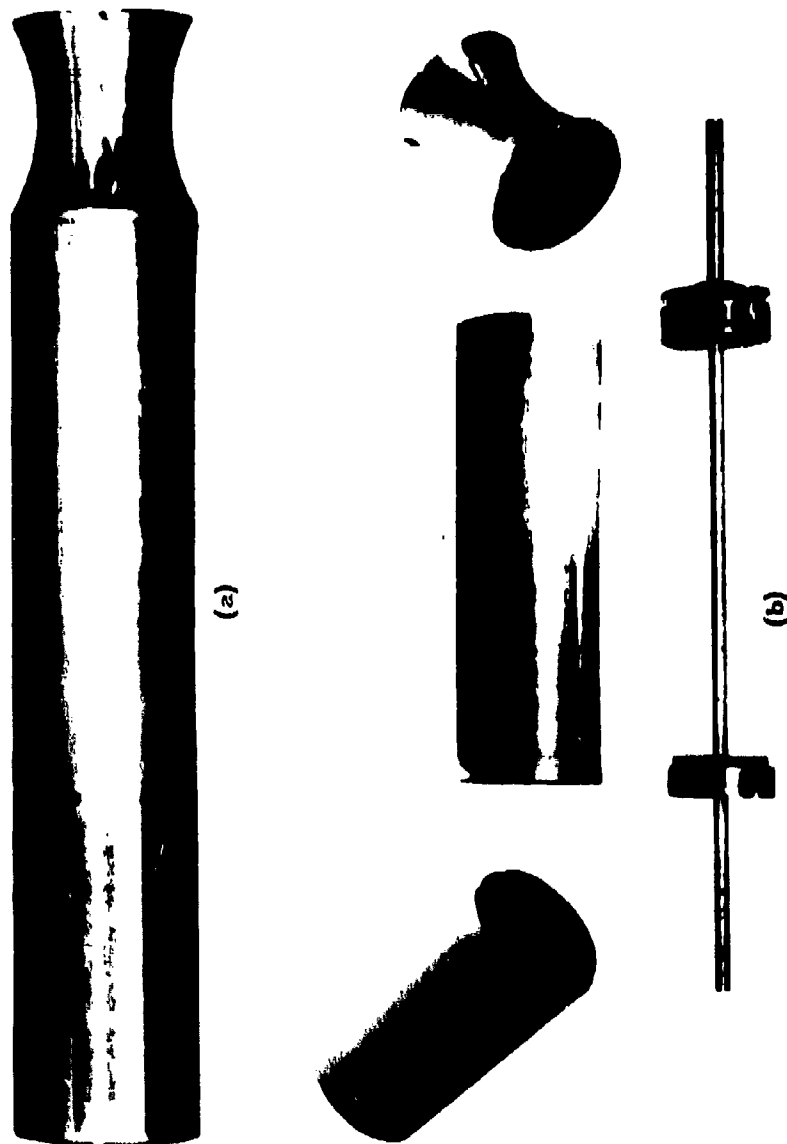


FIG. 14. Dural Disk-Cylinder Missile. (a) Photograph of missile. (b) Exploded view showing structure of aluminum shell and distribution of counterweights.

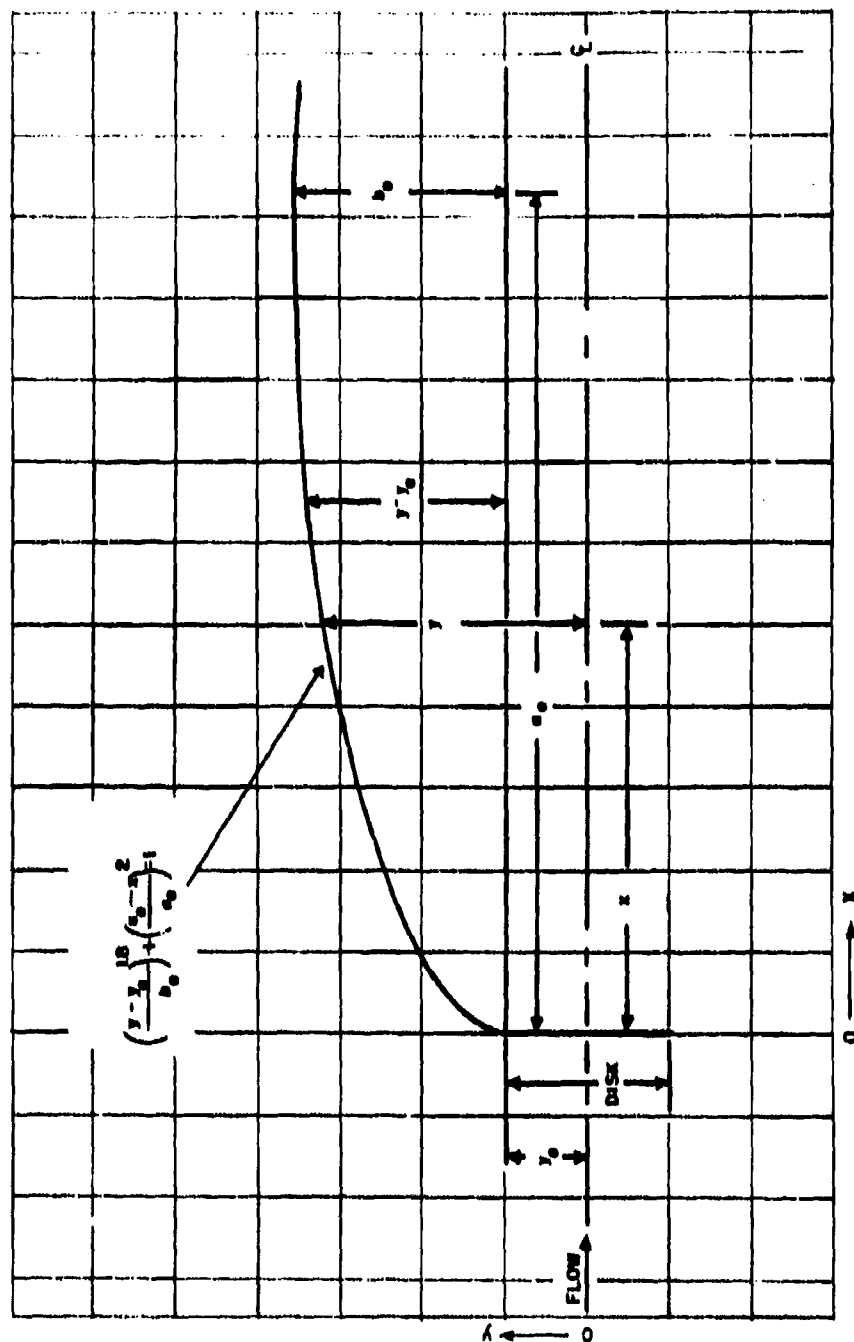


FIG. 15. Definitions of Symbols Used in Eq. 7.

TABLE 6. Two-Inch-Diameter Disk-Cylinder Model Conditions at Which Transient Cavity Data Were Obtained

Launching No., ML	Frame No.	Approx. Depth of Cavity Separation Point, diam.	Approx. Velocity of Missile, fps	Tank Air Press., atm	Cavity
1574	6	18	25	1/27	Open to air
1596	7	24	15	1/27	Open to air
1593	2	8	55	1/2	Closed to air

It might be suspected that the most representative value of σ could be determined from the cavity segment adjacent to the separation point. Unfortunately data from the Free Surface Water Tunnel indicate that this portion of the steady-state cavity is completely independent of σ .

The other alternative is to measure the a_0 and b_0 from the segmented cavity and then calculate the comparable steady-state contour from Eq. 17. These curves and the transient cavity contours which show the previously mentioned scalloping are shown in Fig. 16-18. The transient cavities are more slender than their calculated steady-state counterparts.

The following empirical expression, similar in form to Eq. 17, was determined from the three transient cavity contours.

$$(18) \quad \left(\frac{y - y_0}{b_0} \right)^{1.8} + \left(\frac{a_0 - x}{a_0} \right)^{1.3} = 1$$

where a_0 and b_0 are defined in Fig. 15.

Since the exponent 1.3 was determined from few data, it must be considered an approximate value. However, the curves from Eq. 18 compare well with the measured cavities (Fig. 16-18) even though an equation of this form must necessarily fair out any scallops in the cavity wall. It is interesting to note that close to the separation point the cavities formed at two different air pressures can be described by a single empirical relationship.

It might be concluded from the data presented in Fig. 16-18 alone that transient cavity pressure cannot safely be predicted from steady-state cavity data. However, even more conclusive proof of this is evident from unpublished Free Surface Water Tunnel data presented in Fig. 19. In Fig. 19 the transient cavity

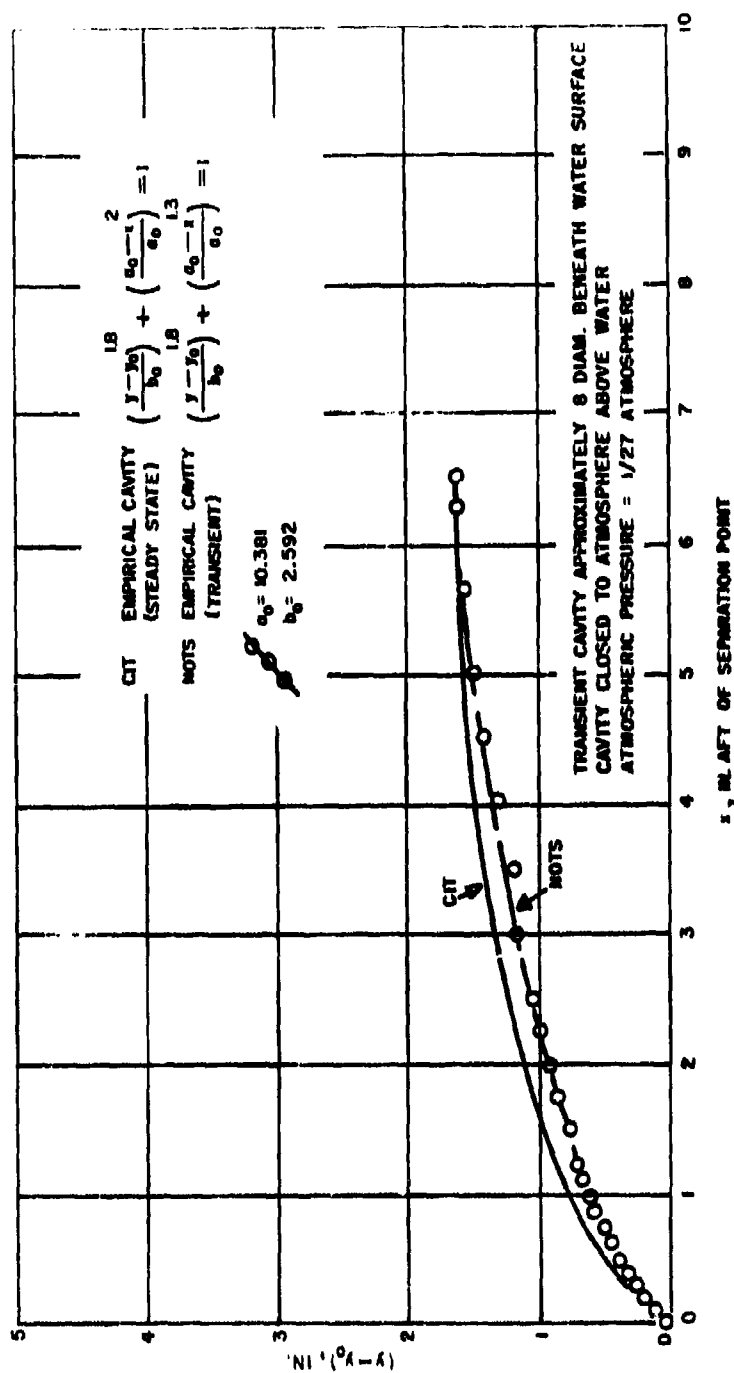


FIG. 16. Comparison of Transient Cavity Contour With Empirical Cavity Shape; a_0 and b_0 Determined From Transient Cavity Shape. Run ML 1593, Frame No. 2.

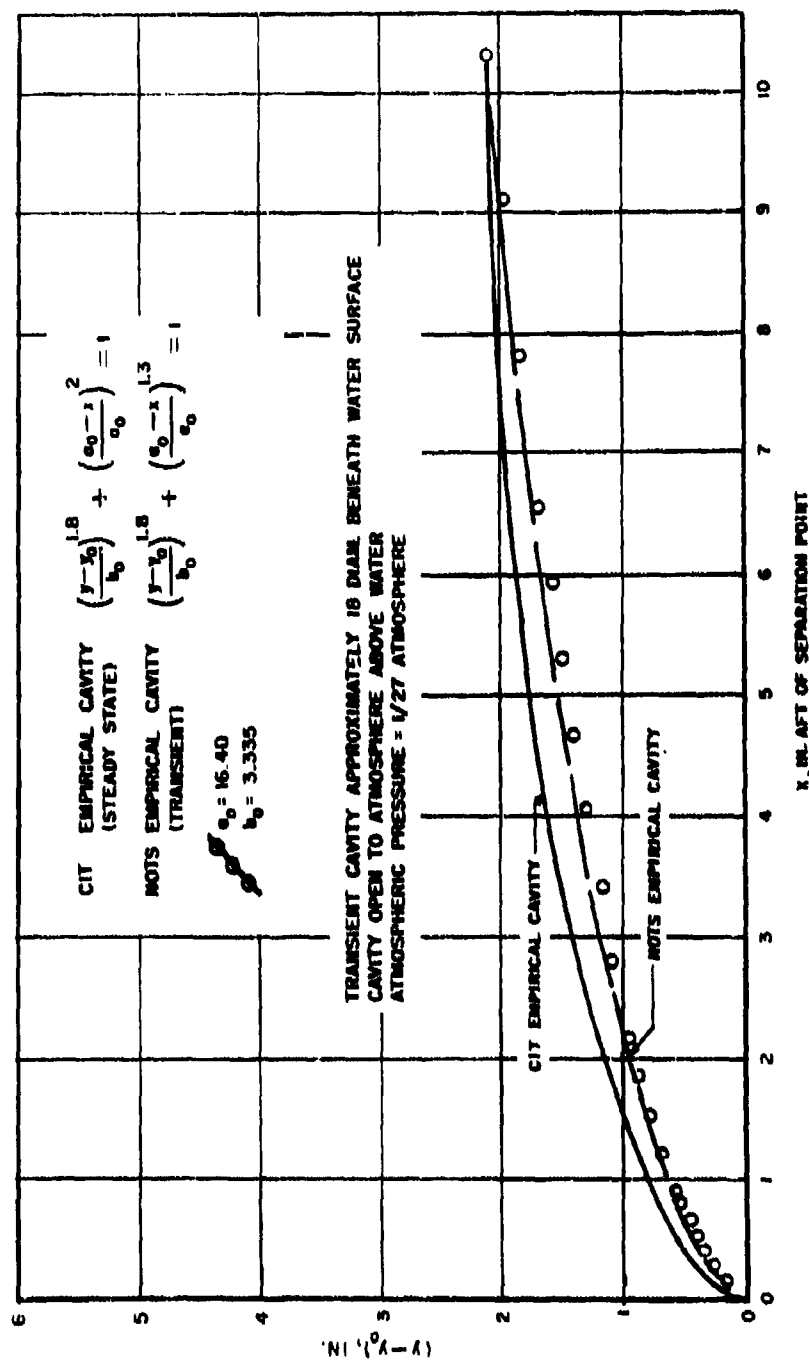


FIG. 17. Comparison of Transient Cavity Contour With Empirical Cavity Shape; a_0 and b_0 Determined From Transient Cavity Shape. Run ML 1574, Frame No. 6.

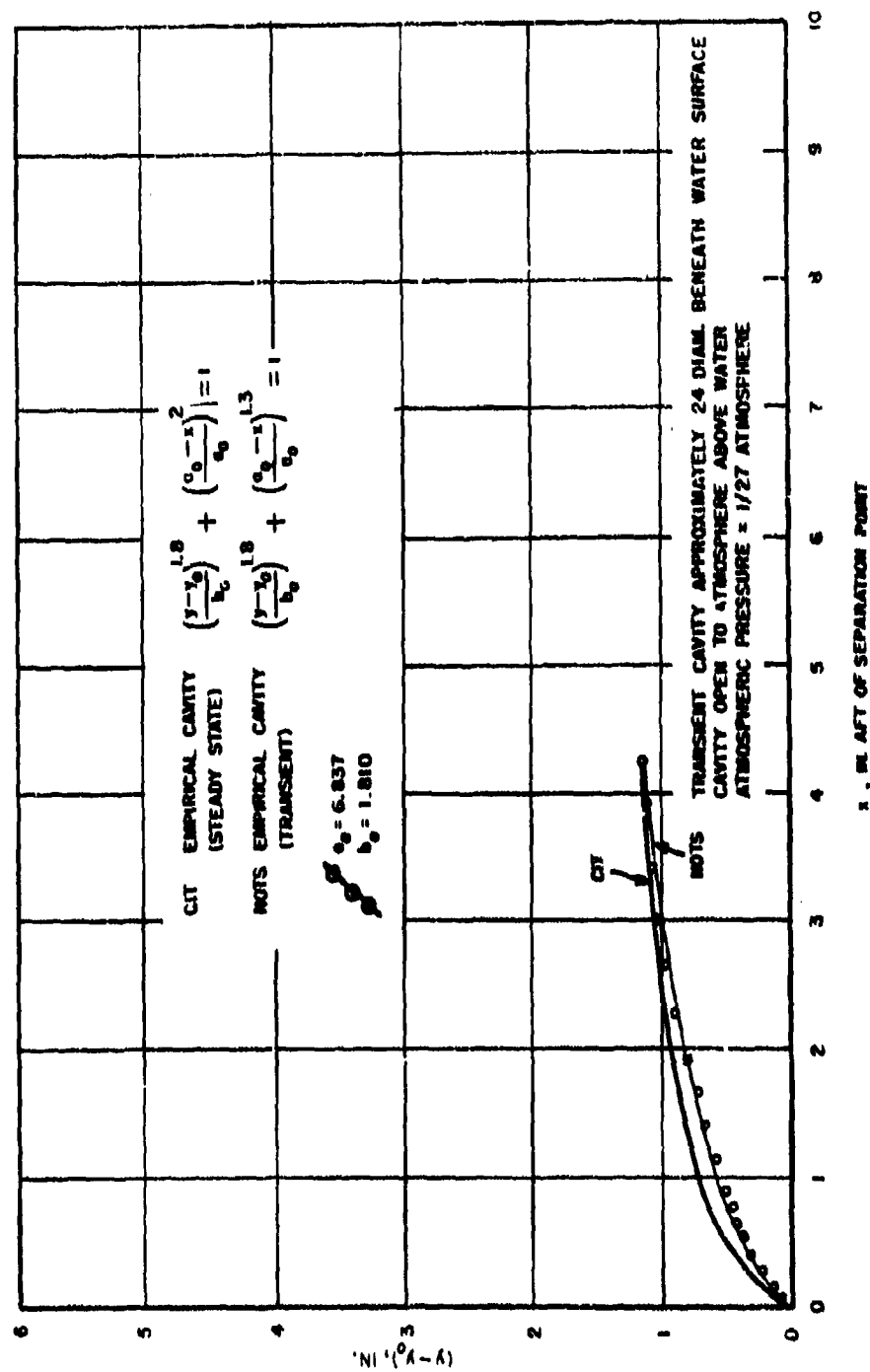


FIG. 18. Comparison of Transient Cavity Contour With Empirical Cavity Shape; a_0 and b_0 Determined From Transient Cavity Shape. Run ML 1596, Frame No. 7.

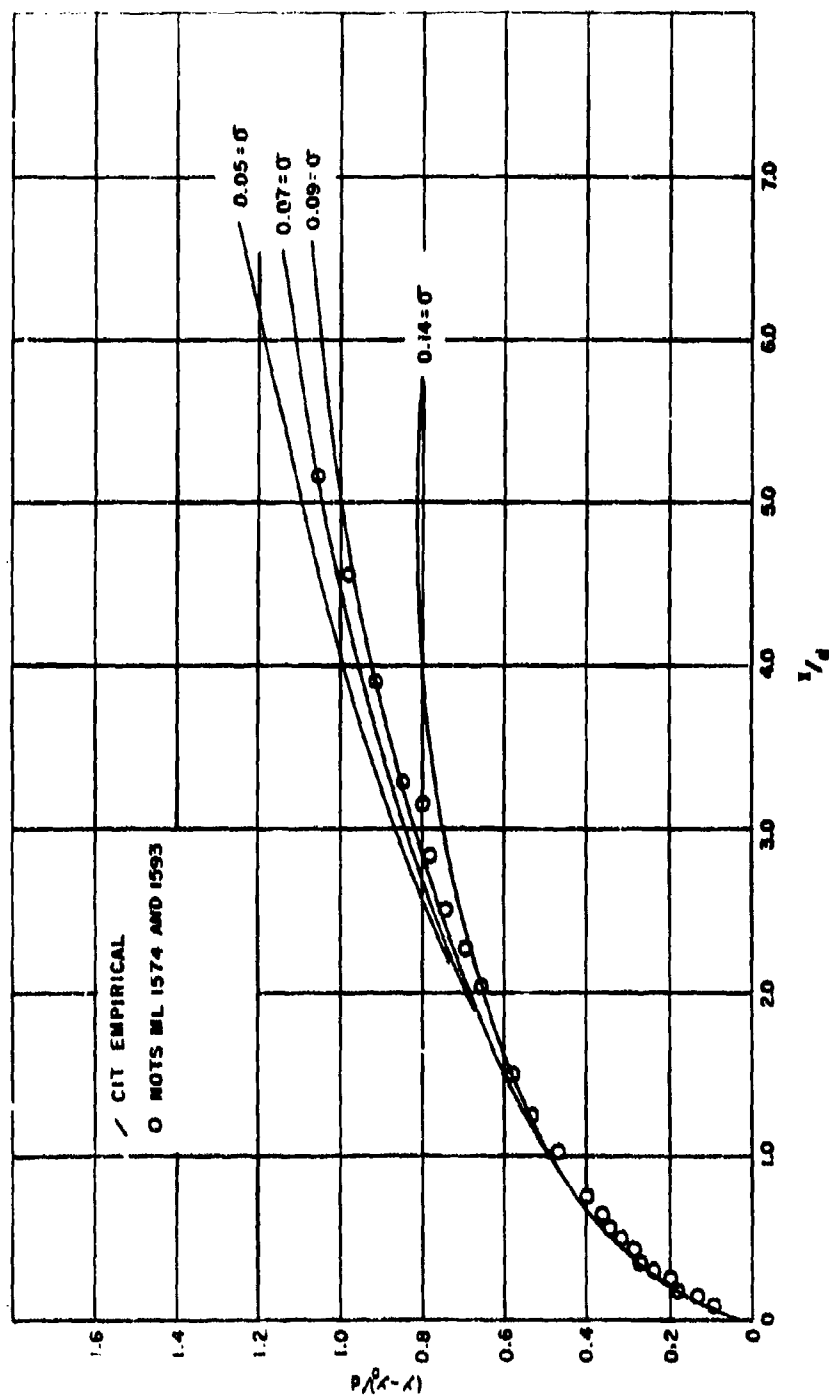


FIG. 19. Comparison of Transient Cavity Contours With Cavity Shapes Measured in CIT Water Tunnel at Various Cavitation Numbers.

contours are compared to the family of steady-state cavities measured at various values of σ between 0.05 and 0.17. Within 1 diameter of the separation point the steady-state cavity contour is independent of σ , and between 1 and 2 diameters aft it is very nearly so. The steady-state cavities begin to show dependence upon cavitation number 2 diameters aft of the separation point. Here the transient data fall upon the steady-state contour $\sigma = 0.14$. Farther aft the σ -contour of best fit decreases with distance from the separation point until at a distance of 5 diameters aft the best fit occurs on the contour $\sigma = 0.07$. This change in σ is too great to be caused by the three-diameter difference in submergence. Hence the data indicate that the internal pressure of the transient cavity cannot be predicted from knowledge of the steady-state cavity.

Appendix B
ORIGIN OF CIRCULAR STRIAE
ON WATER-ENTRY CAVITY

The cavities formed by the disk-cylinder missile (Fig. 14) launched vertically into water with zero angle of attack and 120-fps entry velocity showed well-defined circular striations normal to the direction of missile motion. These striae show clearly in Fig. 20, a typical photograph taken during one of the six duplicate launchings recorded. Birkhoff (Ref. 13) mentions that axial vibration of the missile induced at water entry might cause such striae, but this phenomenon has not previously been observed at this Station.

The longitudinal natural frequency of the missile suspended in air and the frequency at which the striae occurred on the cavity were measured in order to determine whether these striae might be caused by axial vibration of the missile.

The model, suspended from loops of string at the nose and tail, vibrated at a frequency of approximately 2,000 cps when struck sharply upon the flat surface of the nose. The note emitted by the model was measured by matching it to the known tone of a Hewlett-Packard oscillator. The frequency of the striae upon the cavity was estimated as follows from the motion of the missile and the position of the striae with respect to the surface of the water:

1. The velocity of the missile was plotted as a function of distance from the water surface (Fig. 21). (Velocity was determined by numerical differencing of the time-distance data.)
2. The distance of each stria from the water surface was measured and the velocity of the missile at the corresponding point read from the curve (Fig. 21).
3. The time between striae was taken as the distance between striae divided by the average velocity of the missile between the two points at which the striae occurred.

Since the cavity does not remain stationary, only striae within two or three diameters of the missile nose were measured. Separate values of the frequency were determined from each of the first five frames in Fig. 20. The frequency from the first frame was determined from only one measurement, but in the second



FIG. 20. Typical Photograph of Cavity Showing Circular Striations Normal to Direction of Missile Motion.

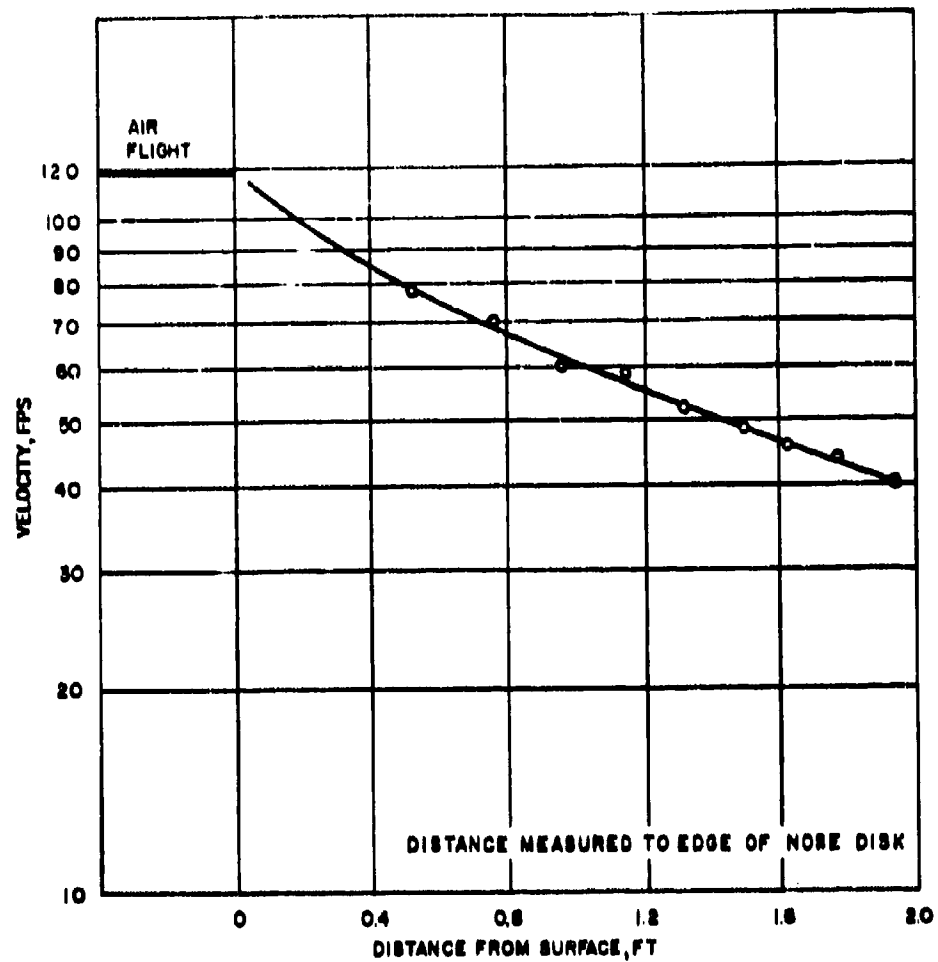


FIG. 21. Velocity of Missile as a Function of Distance Below Water Surface.

through the fifth frames the average of four, five, or seven measurements was used. The scatter in the values averaged was approximately ± 5 percent. The frequency of the cavity striae appeared to increase slightly with time (Fig. 22). Extrapolation of this curve to zero time, which can be estimated only to within $1/2$ ms, gives an initial frequency of 2,250 cps, 12 percent higher than the natural frequency of the missile vibrating in air. Since the difference between the two measured frequencies is of the order of data accuracy, it is quite possible that the striae on the cavity were caused by longitudinal vibration of the missile.

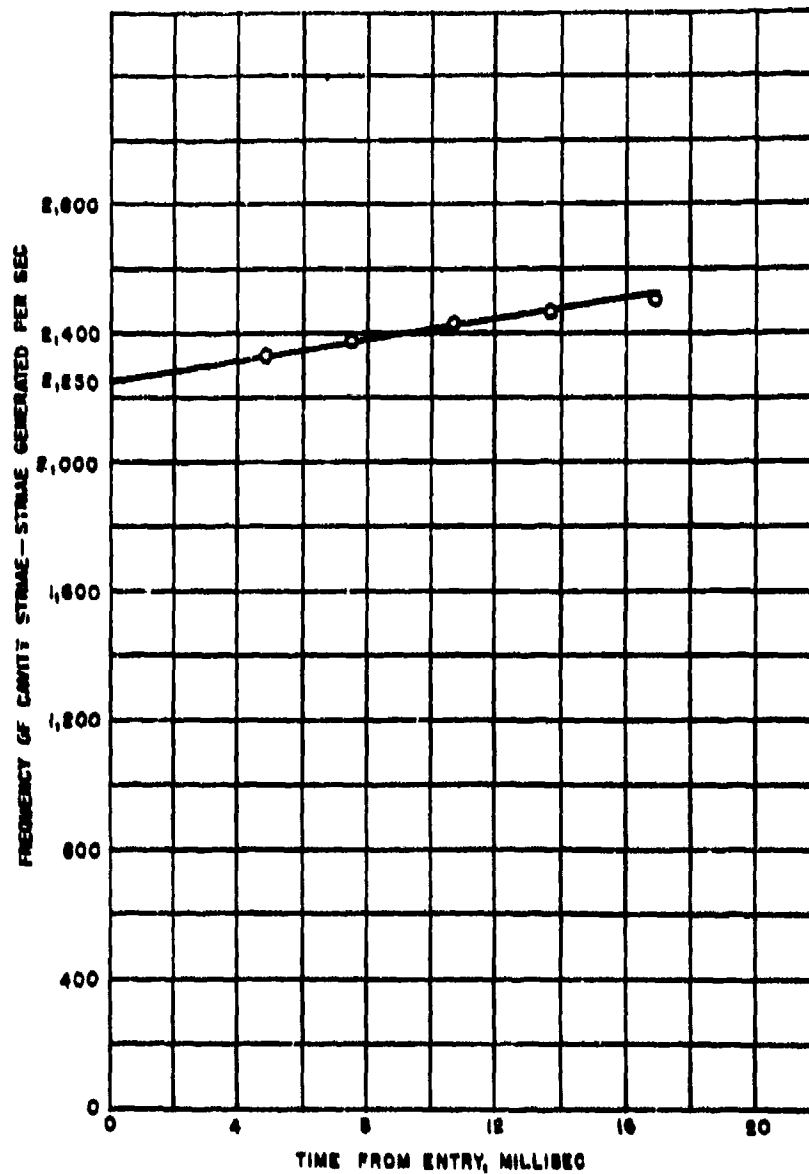


FIG. 22. Frequency of Cavity Striae as a Function of Time From Water Entry.

NOMENCLATURE

D_{\max}	Maximum diameter of cavity containing missile, ft in prototype scale
F	Froude number, $F = v/\sqrt{dg}$
I	Moment of inertia of missile about any transverse axis through the CG, lb in ²
L	Length of cavity containing the missile, ft in prototype scale
R	Reynolds number, $R = vd/\nu$
T	Period of oscillation of cavity diameter, sec in prototype scale
d	Diameter of missile body, in.
g	Acceleration of gravity, ft sec ⁻²
h	Minimum depth of cavity enveloping missile below water surface, ft
l	Distance from nose to CG of missile, in.
m	Mass of missile, lb
p_c	Sum of the gas and vapor pressures in the cavitation bubble acting to keep the bubble open, lb ft ⁻² or atmospheres
p_g	Atmospheric pressure, lb ft ⁻² or atmospheres (standard atmospheric pressure = 740-mm mercury pressure)
$p_g + p_{wgh}$	Sum of the hydrostatic and atmospheric pressures acting to collapse cavitation bubble, lb ft ⁻² . The absolute pressure in the undisturbed liquid, lb ft ⁻² or atmospheres
s	Missile water penetration measured along trajectory from point of water contact, ft
t	Time from instant of missile water contact, sec
v	Velocity of missile, ft sec ⁻¹
v_g	Velocity of gas, ft sec ⁻¹

- α Missile angle of attack in pitch, deg. Angle in the vertical plane between missile axis and direction of motion, positive in the sense of nose-up rotation
- θ Missile angle of pitch, deg. Angle between missile axis and horizontal plane, positive in the sense of nose-up rotation
- λ Modeling scale factor, $\lambda = d_m/d_p$
- ν Kinematic viscosity, $\text{ft}^2 \text{sec}^{-1}$
- ϵ Trajectory angle of missile, deg. Path angle with respect to horizontal plane, positive in climb
- ρ^i Ratio of the density of the gas (irrespective of its associated conditions of temperature and pressure) to that of air at 20°C and 740-mm Hg pressure
- ρ_g Density of gas, slug ft^{-3}
- ρ_w Density of water, slug ft^{-3}
- σ Cavitation number, $\sigma = (p_g + \rho_w g h - p_c) / \frac{1}{2} \rho_w v^2$
- ψ Yaw of missile, deg. Angle between the missile axis and vertical plane containing the trajectory, positive when missile tail is to the right as viewed from the rear
- ω Closure parameter

SUBSCRIPTS

- m Model missiles
- p Prototype missiles

REFERENCES

1. U. S. Naval Ordnance Test Station, Water-Entry Pitch Modeling with One-to-One Froude and Cavitation Number Scaling, by John G. Waugh, China Lake, Calif., NOTS, 8 July 1955. (IDP 22.)
2. California Institute of Technology, Effect of Atmospheric Pressure on Entry Behavior of Models of the Mark 13-6 Torpedo With Standard Head (Head F) and One Finer Head (Head I), by Joseph Levy and John Kaye, Pasadena, Calif., CIT, January 1949. (Hydrodynamics Laboratory Report No. N-59.)
3. ———, Water-Entry Study of the Mk 25 Torpedo with 3.5-Calibre 70-Degree Spherogive Head, by G. M. Wilcox and J. G. Waugh, Pasadena, Calif., CIT, May 1953. (Hydrodynamics Laboratory Report No. E-12.12.)
4. Office of Scientific Research and Development . . . Washington, OSRD, Columbia University, 1946. (Summary technical report of the Applied Mathematics Panel, NDRC, Vol. 1), CONFIDENTIAL.
5. Birkhoff, Garrett, Hydrodynamics, Princeton University Press, 1950.
6. May, Albert, "Vertical Entry of Missiles Into Water," J APPL PHYS, Vol. 23, No. 12 (December 1952), pp. 1362-72.
7. Gilbarg, David, and Robert A. Anderson, "Influence of Atmospheric Pressure on the Phenomena Accompanying the Entry of Spheres into Water," J APPL PHYS, Vol. 19, No. 2 (February 1948), pp. 127-39.
8. U. S. Naval Ordnance Test Station, Inyokern. Article published in Activities of the Underwater Ordnance Department, China Lake, Calif., NOTS, June 1951, CONFIDENTIAL.
9. ———, Laboratory Facilities for Model Studies, by G. G. Mosteller and J. G. Waugh, Inyokern, Calif., NOTS, 14 November 1949. (NAVORD Report 1198, NOTS 254.)
10. ———, Improved Instrumentation for Water-Entry Modeling: Simultaneous Whip and Side-View Photography, by G. G. Mosteller, China Lake, Calif., NOTS, 19 May 1955. (NAVORD Report 3499, NOTS 1125.)

11. E. I. DuPont De Nemours & Company, (Inc.). "Kinetic" Technical Bulletin, "Freon" Compounds. Wilmington, Del., DuPont, 1952.
12. ———. "Kinetic" Technical Bulletin, "Freon" Fluorinated Hydrocarbon Fire Extinguishing Agents. Wilmington, Del., DuPont, 15 November 1954.
13. Bureau of Ordnance. Transient Cavities in Air-Water Entry, by Garrett Birkhoff and Robert Isaacs, Washington, BuOrd, January 1951. (NAVORD Report 1490.)

INITIAL DISTRIBUTION

20 Chief, Bureau of Ordnance

Ad3 (1)
Ad6 (3)
ReO (1)
ReO3 (12)
ReU (1)
ReU1 (1)

**3 Chief of Naval Research
Mechanics Branch (2)**

- 1 Commanding Officer and Director, David W. Taylor Model Basin**
- 1 Commander, Naval Ordnance Laboratory, White Oak**
- 1 Commanding Officer, Naval Underwater Ordnance Station, Newport**
- 1 Commanding Officer, Office of Naval Research, Pasadena**
- 5 Armed Services Technical Information Agency, Dayton**
- 1 Director, Ordnance Research Laboratory, Pennsylvania State University, thru Development Contract Administrator, via InsMat, Reading**
- 2 Director, Hydrodynamics Laboratory, CIT, Pasadena (Mr. Don Price)**

ABSTRACT CARD

U. S. Naval Ordnance Test Station

Water-Entry Cavity Modeling, Part I, Vertical Cavities, by J. G. Waugh and G. W. Stubstad. China Lake, Calif., NOTS, 8 October 1956. 50 pp. (NAVORD Report 5365, Part I; NOTS 1597), UNCLASSIFIED.

ABSTRACT. Modeling studies were conducted with a 2-inch-diameter hemisphere-head missile as a prototype and with 1- and 1/2-inch-diameter models of the prototype. This "modeling with models" program was carried out to investigate

○ (Over)
2 cards, 4 copies

U. S. Naval Ordnance Test Station

Water-Entry Cavity Modeling, Part I, Vertical Cavities, by J. G. Waugh and G. W. Stubstad. China Lake, Calif., NOTS, 8 October 1956. 50 pp. (NAVORD Report 5365, Part I; NOTS 1597), UNCLASSIFIED.

ABSTRACT. Modeling studies were conducted with a 2-inch-diameter hemisphere-head missile as a prototype and with 1- and 1/2-inch-diameter models of the prototype. This "modeling with models" program was carried out to investigate

() (Over)
2 cards, 4 copies

U. S. Naval Ordnance Test Station

Water-Entry Cavity Modeling, Part I, Vertical Cavities, by J. G. Waugh and G. W. Stubstad. China Lake, Calif., NOTS, 8 October 1956. 50 pp. (NAVORD Report 5365, Part I; NOTS 1597), UNCLASSIFIED.

ABSTRACT. Modeling studies were conducted with a 2-inch-diameter hemisphere-head missile as a prototype and with 1- and 1/2-inch-diameter models of the prototype. This "modeling with models" program was carried out to investigate

○ (Over)
2 cards, 4 copies

U. S. Naval Ordnance Test Station

Water-Entry Cavity Modeling, Part I, Vertical Cavities, by J. G. Waugh and G. W. Stubstad. China Lake, Calif., NOTS, 8 October 1956. 50 pp. (NAVORD Report 5365, Part I; NOTS 1597), UNCLASSIFIED.

ABSTRACT. Modeling studies were conducted with a 2-inch-diameter hemisphere-head missile as a prototype and with 1- and 1/2-inch-diameter models of the prototype. This "modeling with models" program was carried out to investigate

() (Over)
2 cards, 4 copies

NAVORD Report 5365

Part I

the importance of gas-density scaling in conjunction with Froude and cavitation-number scaling in water-entry cavity modeling.

The observation of the cavities formed by the vertical entry of these models showed that one-to-one scaling of the Froude and cavitation numbers and of the gas density coefficient modeled the cavity to a high degree of accuracy. Failure to scale the cavitation number did not prevent good modeling, but when the gas density coefficient was not scaled modeling did not occur. Good water-penetration-distance modeling obtained for all modeling

(Contd. on Card 2)

NAVORD Report 5365

Part I

the importance of gas-density scaling in conjunction with Froude and cavitation-number scaling in water-entry cavity modeling.

The observation of the cavities formed by the vertical entry of these models showed that one-to-one scaling of the Froude and cavitation numbers and of the gas density coefficient modeled the cavity to a high degree of accuracy. Failure to scale the cavitation number did not prevent good modeling, but when the gas density coefficient was not scaled modeling did not occur. Good water-penetration-distance modeling obtained for all modeling

(Contd. on Card 2)

NAVORD Report 5365

Part I

the importance of gas-density scaling in conjunction with Froude and cavitation-number scaling in water-entry cavity modeling.

The observation of the cavities formed by the vertical entry of these models showed that one-to-one scaling of the Froude and cavitation numbers and of the gas density coefficient modeled the cavity to a high degree of accuracy. Failure to scale the cavitation number did not prevent good modeling, but when the gas density coefficient was not scaled modeling did not occur. Good water-penetration-distance modeling obtained for all modeling

(Contd. on Card 2)

NAVORD Report 5365

Part I

the importance of gas-density scaling in conjunction with Froude and cavitation-number scaling in water-entry cavity modeling.

The observation of the cavities formed by the vertical entry of these models showed that one-to-one scaling of the Froude and cavitation numbers and of the gas density coefficient modeled the cavity to a high degree of accuracy. Failure to scale the cavitation number did not prevent good modeling, but when the gas density coefficient was not scaled modeling did not occur. Good water-penetration-distance modeling obtained for all modeling

(Contd. on Card 2)

ABSTRACT CARD

U. S. Naval Ordnance Test Station
Water-Entry Cavity . . . (Card 2)

conditions.
Evaluation of the importance of atmospheric density scaling on water-entry modeling must be deferred until tests are extended to include launchings of models at oblique angles.

Cavitation-number scaling cannot be disregarded in the general water-entry modeling problem because it has been found necessary to model missile motion in oblique water entry.



NAVORD Report 5365
Part I

U. S. Naval Ordnance Test Station
Water-Entry Cavity . . . (Card 2)

conditions.
Evaluation of the importance of atmospheric density scaling on water-entry modeling must be deferred until tests are extended to include launchings of models at oblique angles.

Cavitation-number scaling cannot be disregarded in the general water-entry modeling problem because it has been found necessary to model missile motion in oblique water entry.



NAVORD Report 5365
Part I

U. S. Naval Ordnance Test Station
Water-Entry Cavity . . . (Card 2)

conditions.
Evaluation of the importance of atmospheric density scaling on water-entry modeling must be deferred until tests are extended to include launchings of models at oblique angles.

Cavitation-number scaling cannot be disregarded in the general water-entry modeling problem because it has been found necessary to model missile motion in oblique water entry.



NAVORD Report 5365
Part I

U. S. Naval Ordnance Test Station
Water-Entry Cavity . . . (Card 2)

conditions.
Evaluation of the importance of atmospheric density scaling on water-entry modeling must be deferred until tests are extended to include launchings of models at oblique angles.

Cavitation-number scaling cannot be disregarded in the general water-entry modeling problem because it has been found necessary to model missile motion in oblique water entry.



NAVORD Report 5365
Part I

UNCLASSIFIED
AD 128957

Armed Services Technical Information Agency

Reproduced by
DOCUMENT SERVICE CENTER
KNOTT BUILDING, DAYTON, 2, OHIO

This document is the property of the United States Government. It is furnished for the duration of the contract and shall be returned when no longer required, or upon recall by ASTIA to the following address: Armed Services Technical Information Agency, Document Service Center, Knott Building, Dayton 2, Ohio.

NOTICE: WHEN GOVERNMENT OR OTHER DRAWINGS, SPECIFICATIONS, OR OTHER DATA ARE USED FOR ANY PURPOSE OTHER THAN IN CONNECTION WITH A DEFINITELY RELATED GOVERNMENT PROCUREMENT OPERATION, THE U. S. GOVERNMENT THEREBY INCURS NO RESPONSIBILITY, NOR ANY OBLIGATION WHATSOEVER; AND THE FACT THAT THE GOVERNMENT MAY HAVE FORMULATED, FURNISHED, OR IN ANY WAY SUPPLIED THE SAID DRAWINGS, SPECIFICATIONS, OR OTHER DATA IS NOT TO BE REGARDED BY IMPLICATION OR OTHERWISE AS IN ANY MANNER LICENSING THE HOLDER OR ANY OTHER PERSON OR CORPORATION, OR CONVEYING ANY RIGHTS OR PERMISSION TO MANUFACTURE, USE OR SELL ANY PATENTED INVENTION THAT MAY IN ANY WAY BE RELATED THERETO.

UNCLASSIFIED

CLASSIFIED
28957

Armed Services Technical Information Agency

Reproduced by

ARMED SERVICES CENTER

KNOTT BUILDING, DAYTON, 2, OHIO

property of the United States Government. It is furnished for the use of the recipient and shall be returned when no longer required, or upon recall by ASTIA. It is the property of the Armed Services Technical Information Agency, Center, Knott Building, Dayton 2, Ohio.

THIS DOCUMENT OR OTHER DRAWINGS, SPECIFICATIONS, OR OTHER DATA CONTAINED HEREIN ARE TO BE USED ONLY IN CONNECTION WITH A DEFINITELY RELATED GOVERNMENT OPERATION, THE U. S. GOVERNMENT THEREBY INCURS NO LIABILITY OR OBLIGATION WHATSOEVER; AND THE FACT THAT THE INFORMATION IS FORMULATED, FURNISHED, OR IN ANY WAY SUPPLIED THE INFORMATION, OR OTHER DATA IS NOT TO BE REGARDED BY THE RECIPIENT AS IN ANY MANNER LICENSING THIS HOLDER OR ANY OTHER PERSON TO REPRODUCE, IN, OR CONVEYING ANY RIGHTS OR PERMISSION TO MANUFACTURE, OR TO INVENT INVENTION THAT MAY IN ANY WAY BE RELATED THERETO.

CLASSIFIED